Polytopal discontinuous Galerkin discretization of brain multiphysics flow dynamics

Ivan Fumagalli *, Mattia Corti, Nicola Parolini, Paola F. Antonietti

MOX, Department of Mathematics, Politecnico di Milano, piazza Leonardo da Vinci 32, Milan, 20133, Italy

A R T I C L E   I N F O

A B S T R A C T

A comprehensive mathematical model of the multiphysics flow of blood and Cerebrospinal Fluid (CSF) in the brain can be expressed as the coupling of a poromechanics system and Stokes' equations: the first describes fluids filtration through the cerebral tissue and the tissue's elastic response, while the latter models the flow of the CSF in the brain ventricles. This model describes the functioning of the brain's waste clearance mechanism, which has been recently discovered to play an essential role in the progress of neurodegenerative diseases. To model the interactions between different scales in the porous medium, we propose a physically consistent coupling between Multi-compartment Poroelasticity (MPE) equations and Stokes' equations. In this work, we introduce a numerical scheme for the discretization of such coupled MPE-Stokes system, employing a high-order discontinuous Galerkin method on polytopal grids to efficiently account for the geometric complexity of the domain. We analyze the stability and convergence of the space semidiscretized formulation, we prove a-priori error estimates, and we present a temporal discretization based on a combination of Newmark's β-method for the elastic wave equation and the θ-method for the other equations of the model. Numerical simulations carried out on test cases with manufactured solutions validate the theoretical error estimates. We also present numerical results on a two-dimensional slice of a patient-specific brain geometry reconstructed from diagnostic images, to test in practice the advantages of the proposed approach.

1. Introduction

In the brain, multiple fluid components play different roles: the blood supplies nutrients and oxygen and removes carbon dioxide, while the Cerebrospinal Fluid (CSF) and the glymphatic system [1,2] have the primary function of clearing the waste produced by brain activity. Also, it has been recently shown that waste clearance mechanisms play a major role in the evolution of neurodegenerative diseases [3–6]. These physical systems are strongly interconnected with one another and with the cerebral matter: for example, a large amount of the CSF is generated in the choroid plexus thanks to the high concentration of blood capillary vessels in it [7]; also, an auxiliary function of the CSF is to protect the brain from impact against the skull and to compensate blood pulsatility in terms of flow rate and pressure inside the braincase. For this reason, the modeling of the fluid dynamics in the brain requires a multiphysics perspective, able to capture these interactions and their mutual interplay.

From the modeling viewpoint, the brain can be described as a porous material (white and gray matter) with fluids both filtrating through it and flowing in hollow regions (brain ventricles). In terms of mathematical modeling, this can be represented as the coupling

---

* Corresponding author.
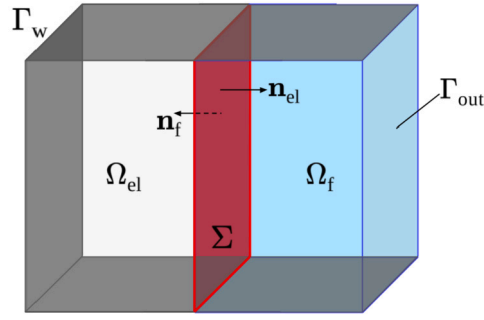*E-mail address:* ivan.fumagalli@polimi.it (I. Fumagalli).

Fig. 1. Domain scheme: poroelastic medium in Ω_{el} (light grey), Stokes' flow of CSF in Ω_f (blue), interface Σ (red), and external boundaries Γ_w (dark grey) and Γ_{out}. (For interpretation of the colors in the figure(s), the reader is referred to the web version of this article.)

between a poromechanics system – described, e.g., by Darcy's or Biot's equations [8] – and Stokes/Navier-Stokes' equations for the flow in the ventricles [9]. Numerical methods for such Fluid-Poroelastic Structure Interaction (FPSI) systems can be found in the literature: the most studied is the Biot-Stokes' system [10–13], but also more complex models have been investigated, e.g. considering a multilayer structure of the porous medium [14,15], a non-linear constitutive model for either the structural or fluid part of the system [16], or Multi-compartment Poroelasticity (MPE) models coupled with Stokes' equations [17,18]. This latter framework is the best suited to model brain poromechanics and CSF flow, since it can simultaneously represent cerebral tissue deformation, blood vessel networks at different scales, CSF flow, and waste clearance. Moreover, the dynamic formulation of MPE equations can describe the inertial forces associated with blood pressure pulsatility during a heartbeat, which affects vascular and tissue deformations and waste clearance [19,20].

The analysis of conforming Finite Element methods for FPSI problems has been addressed in several of the abovementioned works, with a discussion on the inf-sup requirements on the different components of the system (poroelastic, fluid, and coupling conditions). However, aiming at an accurate representation of the poromechanics and flow with low dispersion and dissipation errors, high-order discretization methods provide a better choice [21,22]. Polytopal Discontinuous Galerkin (PolyDG) methods fit in this framework, and they can also naturally account for complex geometries such as vessel networks and brain folds, thanks to their flexibility in terms of local refinement and agglomeration, hanging nodes treatment, and generality of mesh element shapes [23–28]. In addition, discontinuous Galerkin schemes provide a general framework to embed physically-consistent interface conditions directly in the weak form. So far, these methods have been mostly employed to solve porous media and poroelasticity problems for geophysical applications [29–31] and for fluid dynamics and fluid-structure interaction problems [32–37].

In this work, we introduce a high-order PolyDG method to spatially discretize a coupled model encompassing dynamic Multiple-Network Poroelastic (MPE) equations for poromechanics [38] and Stokes' equations [39,40], with physically-consistent coupling conditions inspired from the mass and stress balance at the interface between the brain tissue and the CSF. Moreover, we take full advantage of the DG framework to embed, directly in the physically consistent formulation, the coupling conditions at the interface between the poroelastic and fluid regions. We analyze the well-posedness and convergence of the semidiscrete numerical method, and we employ a combination of Newmark's β-method and the θ-method for time discretization.

The paper is organized as follows. In Section 2, we introduce the multiphysics problem, both in strong and weak form, and discuss the coupling conditions. Section 3 describes the PolyDG space discretization; stability and convergence properties are analyzed in Section 4. Then, time discretization is introduced Section 5. Verification tests are discussed in Section 6, corroborating the theoretical results of Section 4. Section 7 demonstrates the capabilities of the method on a two-dimensional brain section considering physiological settings.

2. Mathematical model

We introduce the mathematical model consisting of the coupling between a Multiple-Network Poroelasticity system and Stokes' system: the former, introduced in [38], accounts for the poromechanics of the brain tissue and its interaction with different fluids compartments flowing in its pores, while the latter describes the flow of the CSF in the brain ventricles. To ease the presentation, we consider a simplified configuration whose two-dimensional representation is depicted in Fig. 1. The poroelastic medium occupies a portion $\Omega_{el} \subset \mathbb{R}^d$ ($d = 2, 3$) of the domain, while the CSF flows according to Stokes' equations in the remaining portion $\Omega_f \subset \mathbb{R}^d$. The interaction between the two systems occurs at the interface $\Sigma = \overline{\Omega}_{el} \cap \overline{\Omega}_f$, which we suppose to be a (piecewise) smooth $(d-1)-$manifold. The source of CSF comes from an exchange of mass with the poroelastic medium and it exits from the domain at Γ_{out}, while the rest of the domain boundary is a solid wall Γ_w. We denote by Ω the interior of $\overline{\Omega}_{el} \cup \overline{\Omega}_f$.

Given a final observation time $T > 0$, we introduce the CSF velocity $\boldsymbol{u} : \Omega_f \times [0, T] \to \mathbb{R}^d$ and pressure $p : \Omega_f \times [0, T] \to \mathbb{R}$, the solid tissue displacement $\boldsymbol{d} : \Omega_{el} \times [0, T] \to \mathbb{R}^d$, and the network pressures $p_j : \Omega_{el} \times [0, T] \to \mathbb{R}$, $j \in J$, where J is a given set of labels denoting the different fluid network compartments [38]. In particular, for the application at hand, we consider $J = \{A, C, V, E\}$, where A, C, V correspond to the arterial, capillary, and venous blood compartments, respectively, while E denotes the extracellular CSF permeating the brain tissue.

Table 1
Parameters of model (1) with corresponding physiological values.

parameter	phys. values	description
ρ_{el}	$1000\,\text{kg} \cdot \text{m}^{-3}$	density of the solid tissue
ρ_f	$1000\,\text{kg} \cdot \text{m}^{-3}$	density of the CSF
μ_{el}	$216\,\text{Pa}$	first Lamé parameter of the solid
λ	$505\,\text{Pa}$	second Lamé parameter of the solid
λ	$11\,567\,\text{Pa}$	second Lamé parameter of the solid [42]
μ_j	$3.5 \cdot 10^{-3}\,\text{Pa} \cdot \text{s}$	viscosity of the fluid in compartment $j \in J$
μ_f	$3.5 \cdot 10^{-3}\,\text{Pa} \cdot \text{s}$	viscosity of CSF
α_j	$\in [0, 1)$	Biot-Willis coefficient of compartment $j \in J$
c_j	$1 \cdot 10^{-6}\,\text{m}^2 \cdot \text{N}^{-1}$	storage coefficient of compartment $j \in J$
k_j	$1 \cdot 10^{-11}\,\text{m}^2$	$K_j = k_j I$ permeability tensor for compartment $j \in J$
k_j	$1 \cdot 10^{-16}\,\text{m}^2$	$K_j = k_j I$ permeability tensor for compartment $j \in J$ [42–44]
β_{jk}	$1\,\text{m}^2 \cdot \text{N}^{-1} \cdot \text{s}^{-1}$	coupling transfer coefficient between compartments (from $k \in J$ to $j \in J$)
β_j^e	$1\,\text{m}^2 \cdot \text{N}^{-1} \cdot \text{s}^{-1}$	external coupling coefficient for compartment $j \in J$

The coupled problem reads as follows:

$$
\begin{cases}
\rho_{el}\partial_{tt}^2 \boldsymbol{d} - \nabla \cdot \sigma_{el}(\boldsymbol{d}) + \sum_{k \in J} \alpha_k \nabla p_k = \boldsymbol{f}_{el}, & \text{in } \Omega_{el} \times (0, T], & \text{(a)} \\
c_j \partial_t p_j + \nabla \cdot \left(\alpha_j \partial_t \boldsymbol{d} - \frac{1}{\mu_j} K_j \nabla p_j \right) & & \\
\quad + \sum_{k \in J} \beta_{jk}(p_j - p_k) + \beta_j^e p_j = g_j, & \text{in } \Omega_{el} \times (0, T], \quad \forall j \in J, & \text{(b)} \\
\rho_f \partial_t \boldsymbol{u} - \nabla \cdot \sigma_f(\boldsymbol{u}) + \nabla p = \boldsymbol{f}_f, & \text{in } \Omega_f \times (0, T], & \text{(c)} \\
\nabla \cdot \boldsymbol{u} = 0, & \text{in } \Omega_f \times (0, T], & \text{(d)}
\end{cases}
\tag{1}
$$

where the linear elastic and fluid (viscous) stress tensors are defined as $\sigma_{el}(\boldsymbol{d}) = 2\mu_{el}\varepsilon(\boldsymbol{d}) + \lambda(\nabla \cdot \boldsymbol{d})I$ and $\sigma_f(\boldsymbol{u}) = 2\mu_f\varepsilon(\boldsymbol{u})$, respectively, with $\varepsilon(\boldsymbol{w}) = (\nabla\boldsymbol{w} + \nabla\boldsymbol{w}^T)/2$. The body forces $\boldsymbol{f}_{el} : \Omega_{el} \times (0, T] \to \mathbb{R}^d, g_j : \Omega_{el} \times (0, T] \to \mathbb{R}, \boldsymbol{f}_f : \Omega_f \times (0, T] \to \mathbb{R}^d$ are supposed sufficiently regular. The parameters of the models are explained in Table 1, with their typical physiological values extracted from [38,41–44]. The initial and boundary conditions of problem (1) are defined as

$$
\begin{cases}
\left(\boldsymbol{d}(0), \partial_t \boldsymbol{d}(0) \right) = \left(\boldsymbol{d}_0, \dot{\boldsymbol{d}}_0 \right), \quad p_j(0) = p_{j0}, & \text{in } \Omega_{el}, \quad \forall j \in J, & \text{(a)} \\
\boldsymbol{u}(0) = \boldsymbol{u}_0 & \text{in } \Omega_f, & \text{(b)} \\
\boldsymbol{d} = \boldsymbol{d}_D = \boldsymbol{0}, & \text{on } \Gamma_w \times (0, T], & \text{(c)} \\
\frac{1}{\mu_j} K_j \nabla p_j \cdot \boldsymbol{n}_{el} = 0, & \text{on } \Gamma_w \times (0, T], \quad \forall j \in J, & \text{(d)} \\
\boldsymbol{u} = \boldsymbol{u}_D = \boldsymbol{0}, & \text{on } \Gamma_w \times (0, T], & \text{(e)} \\
(\sigma_f(\boldsymbol{u}) - pI)\boldsymbol{n}_f = -\overline{p}^{out}\boldsymbol{n}_f, & \text{on } \Gamma_{out} \times (0, T], & \text{(f)}
\end{cases}
\tag{2}
$$

with suitable definition of the data function $\overline{p}^{out} : \Gamma_{out} \times (0, T] \to \mathbb{R}$, that represents the external normal stress at the outlet, and of the initial conditions $\boldsymbol{d}_0 : \Omega_{el} \to \mathbb{R}^d, \dot{\boldsymbol{d}}_0 : \Omega_{el} \to \mathbb{R}^d, \boldsymbol{u}_0 : \Omega_f \to \mathbb{R}^d, p_{j0} : \Omega_{el} \to \mathbb{R}, j \in J$.

On the interface Σ, we introduce the following coupling conditions, based on physiological considerations:

$$
\begin{cases}
\sigma_{el}(\boldsymbol{d})\boldsymbol{n}_{el} - \sum_{k \in J} \alpha_k p_k \boldsymbol{n}_{el} + \sigma_f(\boldsymbol{u})\boldsymbol{n}_f - p\boldsymbol{n}_f = \boldsymbol{0}, & \text{on } \Sigma \times (0, T], & \text{(a)} \\
\frac{1}{\mu_j} K_j \nabla p_j \cdot \boldsymbol{n}_{el} = 0, & \text{on } \Sigma \times (0, T], \quad \forall j \in J \setminus \{E\}, & \text{(b)} \\
\boldsymbol{u} \cdot \boldsymbol{n}_f + \left(\partial_t \boldsymbol{d} - \frac{1}{\mu_E} K_E \nabla p_E \right) \cdot \boldsymbol{n}_{el} = 0, & \text{on } \Sigma \times (0, T], & \text{(c)} \\
p_E = p - \sigma_f(\boldsymbol{u})\boldsymbol{n}_f \cdot \boldsymbol{n}_f, & \text{on } \Sigma \times (0, T], & \text{(d)} \\
\left(\sigma_f(\boldsymbol{u})\boldsymbol{n}_f - p\boldsymbol{n}_f \right) \wedge \boldsymbol{n}_f = \boldsymbol{0}, & \text{on } \Sigma \times (0, T]. & \text{(e)}
\end{cases}
\tag{3}
$$

Condition (3a) expresses the balance of total normal stress. Due to the blood-brain barrier [45,46], we assume that mass exchange between the poroelastic domain and the CSF only occurs through compartment E, as expressed by (3b)-(3c). Consistently, the normal stress of the CSF fluid is balanced by the pressure of compartment E, as in (3d), while we assume the tangential stress on the fluid to be negligible (cf. (3e)). Similar assumptions were made in [42], although we do not make use of the Beavers-Joseph-Saffman condition [47].

Aiming at solving problem (1) with the Finite Element method, we introduce its weak formulation. For the sake of generality, let $\Gamma_{D,\boldsymbol{d}}, \Gamma_{D,\boldsymbol{u}}, \Gamma_{D,P_j}$, with $j \in J$, denote the portions of $\partial\Omega$ where Dirichlet boundary conditions on $\boldsymbol{d}, \boldsymbol{u}, p_j$ are imposed, respectively. Then, we introduce the following functional spaces:

$$
\boldsymbol{W} = \{\boldsymbol{w} \in [H^1(\Omega_{el})]^d : \boldsymbol{w} = 0 \text{ on } \Gamma_{D,\boldsymbol{d}}\}, \qquad \boldsymbol{V} = \{\boldsymbol{v} \in [H^1(\Omega_f)]^d : \boldsymbol{v} = 0 \text{ on } \Gamma_{D,\boldsymbol{u}}\},
$$

$$
Q_j = \{q_j \in H^1(\Omega_{el}) : q_j = 0 \text{ on } \Gamma_{D,P_j}\}, \; \forall j \in J, \qquad Q = L^2(\Omega_f),
$$

where $H^1(\Omega)$ denotes the classical Sobolev space of order 1 over $L^2(\Omega)$. For the problem at hand, all Dirichlet boundary conditions on $\partial\Omega$ are homogeneous. We denote by $(\cdot,\cdot)_\Omega$ the L^2-product over Ω and we define the following forms and functionals over the spaces introduced above:

$$a_{\mathrm{el}} : \boldsymbol{W} \times \boldsymbol{W} \to \mathbb{R}, \quad a_{\mathrm{el}}(\boldsymbol{d},\boldsymbol{w}) = (\sigma_{\mathrm{el}}(\boldsymbol{d}), \varepsilon(\boldsymbol{w}))_{\Omega_{\mathrm{el}}},$$

$$a_{\mathrm{j}} : Q_{\mathrm{j}} \times Q_{\mathrm{j}} \to \mathbb{R}, \quad a_{\mathrm{j}}(p_{\mathrm{j}}, q_{\mathrm{j}}) = \left(\frac{1}{\mu_{\mathrm{j}}} K_{\mathrm{j}} \nabla p_{\mathrm{j}}, \nabla q_{\mathrm{j}}\right)_{\Omega_{\mathrm{el}}} \quad \forall \mathrm{j} \in J,$$

$$C_{\mathrm{j}} : \left(\bigtimes_{\mathrm{k} \in J} Q_{\mathrm{k}}\right) \times Q_{\mathrm{j}} \to \mathbb{R}, \quad C_{\mathrm{j}}(\{p_{\mathrm{k}}\}_{\mathrm{k} \in J}, q_{\mathrm{j}}) = \sum_{\mathrm{k} \in J} (\beta_{\mathrm{kj}}(p_{\mathrm{j}} - p_{\mathrm{k}}), q_{\mathrm{j}})_{\Omega_{\mathrm{el}}} + (\beta_{\mathrm{j}}^{\mathrm{e}} p_{\mathrm{j}}, q_{\mathrm{j}})_{\Omega_{\mathrm{el}}} \quad \forall \mathrm{j} \in J,$$

$$a_{\mathrm{f}} : \boldsymbol{V} \times \boldsymbol{V} \to \mathbb{R}, \quad a_{\mathrm{f}}(\boldsymbol{u},\boldsymbol{v}) = (\sigma_{\mathrm{f}}(\boldsymbol{u}), \varepsilon(\boldsymbol{v}))_{\Omega_{\mathrm{f}}},$$

$$b_{\mathrm{j}} : Q_{\mathrm{j}} \times \boldsymbol{W} \to \mathbb{R}, \quad b_{\mathrm{j}}(q_{\mathrm{j}}, \boldsymbol{w}) = -(\alpha_{\mathrm{j}} p_{\mathrm{j}}, \mathrm{div}\,\boldsymbol{w})_{\Omega_{\mathrm{el}}} \quad \forall \mathrm{j} \in J,$$

$$b_{\mathrm{f}} : Q \times \boldsymbol{V} \to \mathbb{R}, \quad b_{\mathrm{f}}(q,\boldsymbol{v}) = -(q, \mathrm{div}\,\boldsymbol{v})_{\Omega_{\mathrm{f}}},$$

$$F_{\mathrm{el}} : \boldsymbol{W} \to \mathbb{R}, \quad F_{\mathrm{el}}(\boldsymbol{w}) = (\boldsymbol{f}_{\mathrm{el}}, \boldsymbol{w})_{\Omega_{\mathrm{el}}},$$

$$F_{\mathrm{j}} : Q_{\mathrm{j}} \to \mathbb{R}, \quad F_{\mathrm{j}}(q_{\mathrm{j}}) = (g_{\mathrm{j}}, q_{\mathrm{j}})_{\Omega_{\mathrm{el}}} \quad \forall \mathrm{j} \in J,$$

$$F_{\mathrm{f}} : \boldsymbol{V} \to \mathbb{R}, \quad F_{\mathrm{f}}(\boldsymbol{v}) = (\boldsymbol{f}_{\mathrm{f}}, \boldsymbol{v})_{\Omega_{\mathrm{f}}},$$

$$\mathfrak{F} : Q_{\mathrm{E}} \times \boldsymbol{W} \times \boldsymbol{V} \to \mathbb{R}, \quad \mathfrak{F}(p_{\mathrm{E}}, \boldsymbol{w}, \boldsymbol{v}) = \int_\Sigma p_{\mathrm{E}} \left(\boldsymbol{w} \cdot \boldsymbol{n}_{\mathrm{el}} + \boldsymbol{v} \cdot \boldsymbol{n}_{\mathrm{f}}\right) d\Sigma.$$

Remark 1 (*Derivation of the interface form* $\mathfrak{F}$). The interface form $\mathfrak{F} : Q_{\mathrm{E},h}^{\mathrm{DG}} \times \boldsymbol{W}_h^{\mathrm{DG}} \times \boldsymbol{V}_h^{\mathrm{DG}} \to \mathbb{R}$ introduced above naturally arises during the derivation of the weak form of problem (1). We test (1a)-(1b) against functions $\boldsymbol{w} \in \boldsymbol{W}$ and $q_{\mathrm{j}} \in Q_{\mathrm{j}}$, with $\mathrm{j} \in J$, over Ω_{el}, and (1c) against $\boldsymbol{v} \in \boldsymbol{V}$ over Ω_{f}. Then, integrating by parts and summing all the contributions yield the following boundary terms on the interface:

$$\int_\Sigma \left[(pI - \sigma_{\mathrm{f}}(\boldsymbol{u})) : \boldsymbol{v} \otimes \boldsymbol{n}_{\mathrm{f}} + \left(\sum_{\mathrm{k} \in J} \alpha_{\mathrm{k}} p_{\mathrm{k}} I - \sigma_{\mathrm{el}}(\boldsymbol{d})\right) : \boldsymbol{w} \otimes \boldsymbol{n}_{\mathrm{el}} - \sum_{\mathrm{j} \in J} \frac{1}{\mu_{\mathrm{j}}} K_{\mathrm{j}} \nabla p_{\mathrm{j}} \cdot q_{\mathrm{j}} \boldsymbol{n}_{\mathrm{el}} \right] d\Sigma. \tag{4}$$

Using the interface conditions (3a)-(3b) and then (3c)-(3d)-(3e), we can rewrite (4) as follows:

$$\int_\Sigma \left[(pI - \sigma_{\mathrm{f}}(\boldsymbol{u})) : (\boldsymbol{v} \otimes \boldsymbol{n}_{\mathrm{f}} + \boldsymbol{w} \otimes \boldsymbol{n}_{\mathrm{el}}) - \frac{1}{\mu_{\mathrm{E}}} K_{\mathrm{E}} \nabla p_{\mathrm{E}} \cdot q_{\mathrm{E}} \boldsymbol{n}_{\mathrm{el}} \right] d\Sigma$$

$$= \int_\Sigma \left[p_{\mathrm{E}}(\boldsymbol{v} \cdot \boldsymbol{n}_{\mathrm{f}} + \boldsymbol{w} \cdot \boldsymbol{n}_{\mathrm{el}}) - q_{\mathrm{E}}(\boldsymbol{u} \cdot \boldsymbol{n}_{\mathrm{f}} + \partial_t \boldsymbol{d} \cdot \boldsymbol{n}_{\mathrm{el}}) \right] d\Sigma = \mathfrak{F}(p_{\mathrm{E}}, \boldsymbol{w}, \boldsymbol{v}) - \mathfrak{F}(q_{\mathrm{E}}, \partial_t \boldsymbol{d}, \boldsymbol{u}), \tag{5}$$

where we also used that $\boldsymbol{a} \otimes \boldsymbol{b} : I = \boldsymbol{a} \cdot \boldsymbol{b}$ for any $\boldsymbol{a}, \boldsymbol{b} \in \mathbb{R}^d$.

Denoting by $L^2(0,T;H), H^1(0,T;H)$ the time-dependent Bochner spaces associated to a Sobolev space H, and setting

$$\mathscr{D} = H^2(0,T;\boldsymbol{W}), \quad \mathscr{P} = \bigtimes_{\mathrm{j} \in J} H^1(0,T;Q_{\mathrm{j}}), \quad \mathscr{V} = H^1(0,T;\boldsymbol{V}), \quad \mathscr{Q} = L^2(0,T;Q),$$

the weak formulation of problem (1) reads as follows:
Find $(\boldsymbol{d}, \{p_{\mathrm{j}}\}_{\mathrm{j} \in J}, \boldsymbol{u}, p) \in \mathscr{D} \times \mathscr{P} \times \mathscr{V} \times \mathscr{Q}$ such that, for all $t \in (0,T]$,

$$(\rho_{\mathrm{el}} \partial_{tt}^2 \boldsymbol{d}, \boldsymbol{w})_{\Omega_{\mathrm{el}}} + a_{\mathrm{el}}(\boldsymbol{d}, \boldsymbol{w}) + \sum_{\mathrm{j} \in J} b_{\mathrm{j}}(p_{\mathrm{j}}, \boldsymbol{w}) - F_{\mathrm{el}}(\boldsymbol{w})$$

$$+ \sum_{\mathrm{j} \in J} \left[(c_{\mathrm{j}} \partial_t p_{\mathrm{j}}, q_{\mathrm{j}})_{\Omega_{\mathrm{el}}} + a_{\mathrm{j}}(p_{\mathrm{j}}, q_{\mathrm{j}}) + C_{\mathrm{j}}(\{p_{\mathrm{k}}\}_{\mathrm{k} \in J}, q_{\mathrm{j}}) - b_{\mathrm{j}}(q_{\mathrm{j}}, \partial_t \boldsymbol{d}) - F_{\mathrm{j}}(q_{\mathrm{j}}) \right]$$

$$+ (\rho_{\mathrm{f}} \partial_t \boldsymbol{u}, \boldsymbol{v})_{\Omega_{\mathrm{f}}} + a_{\mathrm{f}}(\boldsymbol{u}, \boldsymbol{v}) + b_{\mathrm{f}}(p, \boldsymbol{v}) + b_{\mathrm{f}}(q, \boldsymbol{u}) - F_{\mathrm{f}}(\boldsymbol{v})$$

$$+ \mathfrak{F}(p_{\mathrm{E}}, \boldsymbol{w}, \boldsymbol{v}) - \mathfrak{F}(q_{\mathrm{E}}, \partial_t \boldsymbol{d}, \boldsymbol{u}) = 0 \tag{6}$$

for all $(\boldsymbol{w}, \{q_{\mathrm{j}}\}_{\mathrm{j} \in J}, \boldsymbol{v}, q) \in \mathscr{D} \times \mathscr{P} \times \mathscr{V} \times \mathscr{Q}$, and $\boldsymbol{d}(0) = \boldsymbol{d}_0, \partial_t \boldsymbol{d}(0) = \dot{\boldsymbol{d}}_0, \boldsymbol{u}(0) = \boldsymbol{u}_0, p_{\mathrm{j}}(0) = p_{\mathrm{j}0} \; \forall \mathrm{j} \in J$.

3. Semidiscrete formulation based on a polytopal discontinuous Galerkin method

In this section, we introduce a space discretization of problem (6) based on discontinuous Finite Element methods on polytopal grids.
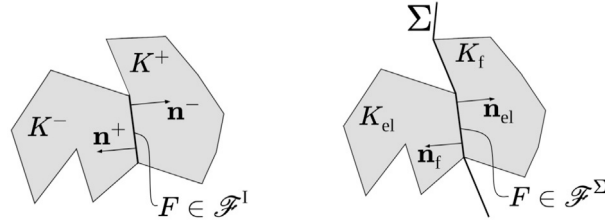
Fig. 2. Polygonal elements sharing an internal face (left) or a face on the interface Σ (right).

3.1. Notation

Let $\mathscr{T}_{h,\mathrm{el}}, \mathscr{T}_{h,\mathrm{f}}$ be polytopal meshes discretizing the domains $\Omega_{\mathrm{el}}, \Omega_{\mathrm{f}}$, respectively. We define as *faces* of an element $K \in \mathscr{T}_{h,\mathrm{el}} \cup \mathscr{T}_{h,\mathrm{f}}$ the $(d-1)$-dimensional entities corresponding to the intersection of ∂K with either the boundary of a neighboring element or the domain boundary $\partial \Omega$:

- for $d = 2$, the faces are always straight line segments;
- for $d = 3$, the faces are generic polygons. We assume that each face can be decomposed into triangles.

With this definition, we denote by $\mathscr{F}_{\mathrm{el}}, \mathscr{F}_{\mathrm{f}}$ the sets of element faces corresponding to each physical domain. We partition them into internal faces $\mathscr{F}_{\mathrm{el}}^{\mathrm{I}}, \mathscr{F}_{\mathrm{f}}^{\mathrm{I}}$, Dirichlet/Neumann faces $\mathscr{F}_{\mathrm{el}}^{\mathrm{D}}/\mathscr{F}_{\mathrm{el}}^{\mathrm{N}} \subset \partial\Omega_{\mathrm{el}} \setminus \Sigma, \mathscr{F}_{\mathrm{el}}^{\mathrm{D_j}}/F_{\mathrm{el}}^{\mathrm{N_j}} \subset \partial\Omega_{\mathrm{el}} \setminus \Sigma, \mathscr{F}_{\mathrm{f}}^{\mathrm{D}}/\mathscr{F}_{\mathrm{f}}^{\mathrm{N}} \subset \partial\Omega_{\mathrm{f}} \setminus \Sigma$ (for the elastic displacement, the pressure of the j-th compartment, and the fluid velocity, respectively), and interface faces $\mathscr{F}^{\Sigma} \subset \Sigma$. In the latter, we assume that the meshes $\mathscr{T}_{h,\mathrm{el}}, \mathscr{T}_{h,\mathrm{f}}$ are aligned with Σ, namely that there is no gap or overlap between them, although hanging nodes are permitted.

We introduce the symmetric outer product $\boldsymbol{v} \odot \boldsymbol{n} = \frac{1}{2}(\boldsymbol{v} \otimes \boldsymbol{n} + \boldsymbol{n} \otimes \boldsymbol{v})$ and, for regular enough scalar-, vector- and tensor-valued functions $q, \boldsymbol{v}, \tau$, we define the following average and jump operators:

- On each internal face $F \in \mathscr{F}^{\mathrm{I}} = \mathscr{F}_{\mathrm{el}}^{\mathrm{I}} \cup \mathscr{F}_{\mathrm{f}}^{\mathrm{I}}$ we set

$$\{\!\{q\}\!\} = \frac{1}{2}(q^+ + q^-), \qquad \{\!\{\boldsymbol{v}\}\!\} = \frac{1}{2}(\boldsymbol{v}^+ + \boldsymbol{v}^-), \qquad \{\!\{\tau\}\!\} = \frac{1}{2}(\tau^+ + \tau^-),$$

$$[\![q]\!] = q^+ \boldsymbol{n}^+ + q^- \boldsymbol{n}^-, \qquad [\![\boldsymbol{v}]\!] = \boldsymbol{v}^+ \odot \boldsymbol{n}^+ + \boldsymbol{v}^- \odot \boldsymbol{n}^-, \qquad [\![\tau]\!] = \tau^+ \boldsymbol{n}^+ + \tau^- \boldsymbol{n}^-,$$

where $\boldsymbol{n}^+, \boldsymbol{n}^-$ are defined as in Fig. 2 - left.

- On a Dirichlet face $F \in \mathscr{F}_{\mathrm{el}}^{\mathrm{D}} \cup \left(\bigcup_{\mathrm{j} \in J} \in \mathscr{F}_{\mathrm{el}}^{\mathrm{D_j}} \right) \cup \mathscr{F}_{\mathrm{f}}^{\mathrm{D}}$:

$$\{\!\{q\}\!\} = q, \qquad \{\!\{\boldsymbol{v}\}\!\} = \boldsymbol{v}, \qquad \{\!\{\tau\}\!\} = \tau,$$

$$[\![q]\!] = q\boldsymbol{n}, \qquad [\![\boldsymbol{v}]\!] = \boldsymbol{v} \odot \boldsymbol{n}, \qquad [\![\tau]\!] = \tau\boldsymbol{n},$$

where $\boldsymbol{n}$ is the unit normal vector pointing outward to the element K to which the face F belongs.

- On a face $F \in \mathscr{F}^{\Sigma}$ shared by two elements $K_{\mathrm{el}} \in \mathscr{T}_{h,\mathrm{el}}$ and $K_{\mathrm{f}} \in \mathscr{T}_{h,\mathrm{f}}$:

$$\{\!\{q\}\!\} = q|_{K_{\mathrm{el}}}, \qquad \{\!\{\tau\}\!\} = \tau|_{K_{\mathrm{el}}}, \qquad [\![\boldsymbol{w}, \boldsymbol{v}]\!] = \boldsymbol{w}|_{K_{\mathrm{el}}} \odot \boldsymbol{n}_{\mathrm{el}} + \boldsymbol{v}|_{K_{\mathrm{f}}} \odot \boldsymbol{n}_{\mathrm{f}},$$

where $\boldsymbol{n}_{\mathrm{el}}, \boldsymbol{n}_{\mathrm{f}}$ are defined as in Fig. 2 - right.

3.2. PolyDG semidiscrete problem

For a given integer $m \geq 1$, we introduce the following piecewise polynomial spaces:

$$X_h^{\mathrm{DG}}(\Omega_{\star}) = \{\phi \in L^2(\Omega_{\star}) : \phi|_K \in \mathbb{P}^m(K) \quad \forall K \in \mathscr{T}_{\star}\}, \qquad \star = \mathrm{el}, \mathrm{f}$$

$$Q_{\mathrm{j},h}^{\mathrm{DG}} = X_h^{\mathrm{DG}}(\Omega_{\mathrm{el}}), \quad Q_h^{\mathrm{DG}} = X_h^{\mathrm{DG}}(\Omega_{\mathrm{f}}), \quad \boldsymbol{W}_h^{\mathrm{DG}} = [X_h^{\mathrm{DG}}(\Omega_{\mathrm{el}})]^d, \quad \boldsymbol{V}_h^{\mathrm{DG}} = [X_h^{\mathrm{DG}}(\Omega_{\mathrm{f}})]^d.$$

Moreover, we denote by $H^s(\mathscr{T}_{\mathrm{el}}), H^s(\mathscr{T}_{\mathrm{f}})$ the broken Sobolev spaces of order s over the mesh of the poroelastic and fluid domains, namely $H^s(\mathscr{T}_{\star}) = \{q \in L^2(\Omega_{\star}) : q|_K \in H^s(K) \quad \forall K \in \mathscr{T}_{\star}\}$ for $\star = \mathrm{el}, \mathrm{f}$. We then introduce the following forms, for $\boldsymbol{d}, \boldsymbol{w} \in [H^1(\mathscr{T}_{h,\mathrm{el}})]^d, p_{\mathrm{j}}, q_{\mathrm{j}} \in H^1(\mathscr{T}_{h,\mathrm{el}})$, with $\mathrm{j} \in J, \boldsymbol{u}, \boldsymbol{v} \in [H^1(\mathscr{T}_{h,\mathrm{f}})]^d, p, q \in H^1(\mathscr{T}_{h,\mathrm{f}})$:

$$\mathcal{A}_{\mathrm{el}}(\boldsymbol{d}, \boldsymbol{w}) = \int_{\Omega_{\mathrm{el}}} \sigma_{\mathrm{el}}(\boldsymbol{d}) : \varepsilon_h(\boldsymbol{w}) - \sum_{F \in \mathscr{F}_{\mathrm{el}}^{\mathrm{I}} \cup \mathscr{F}_{\mathrm{el}}^{\mathrm{D}}} \int_F \left(\{\!\{\sigma_{\mathrm{el}}(\boldsymbol{d})\}\!\} : [\![\boldsymbol{w}]\!] + [\![\boldsymbol{d}]\!] : \{\!\{\sigma_{\mathrm{el}}(\boldsymbol{w})\}\!\} - \eta[\![\boldsymbol{d}]\!] : [\![\boldsymbol{w}]\!] \right), \tag{7a}$$

$$\mathcal{F}_{\mathrm{el}}(\boldsymbol{w}) = \int_{\Omega_{\mathrm{el}}} \boldsymbol{f}_{\mathrm{el}} \cdot \boldsymbol{w}, \tag{7b}$$

$$\mathcal{B}_{\mathrm{j}}(p_{\mathrm{j}}, \boldsymbol{w}) = -\int_{\Omega_{\mathrm{el}}} \alpha_{\mathrm{j}} p_{\mathrm{j}} \operatorname{div}_h \boldsymbol{w} + \sum_{F \in \mathscr{F}_{\mathrm{el}}^{\mathrm{I}} \cup \mathscr{F}_{\mathrm{el}}^{\mathrm{D}_{\mathrm{j}}}} \int_F \alpha_{\mathrm{j}} \{\!\{ p_{\mathrm{j}} I \}\!\} : [\![\boldsymbol{w}]\!], \tag{7c}$$

$$\mathcal{A}_{\mathrm{j}}(p_{\mathrm{j}}, q_{\mathrm{j}}) = \int_{\Omega_{\mathrm{el}}} \mu_{\mathrm{j}}^{-1} K_{\mathrm{j}} \nabla_h p_{\mathrm{j}} \cdot \nabla_h q_{\mathrm{j}} - \sum_{F \in \mathscr{F}_{\mathrm{el}}^{\mathrm{I}} \cup \mathscr{F}_{\mathrm{el}}^{\mathrm{D}_{\mathrm{j}}}} \int_F \left(\{\!\{ \mu_{\mathrm{j}}^{-1} K_{\mathrm{j}} \nabla_h p_{\mathrm{j}} \}\!\} \cdot [\![q_{\mathrm{j}}]\!] + [\![p_{\mathrm{j}}]\!] \cdot \{\!\{ \mu_{\mathrm{j}}^{-1} K_{\mathrm{j}} \nabla_h q_{\mathrm{j}} \}\!\} - \zeta_{\mathrm{j}} [\![p_{\mathrm{j}}]\!] \cdot [\![q_{\mathrm{j}}]\!] \right), \tag{7d}$$

$$C_{\mathrm{j}}(\{p_{\mathrm{k}}\}_{\mathrm{k} \in J}, q_{\mathrm{j}}) = \int_{\Omega_{\mathrm{el}}} \sum_{\mathrm{k} \in J} \beta_{\mathrm{kj}} (p_{\mathrm{j}} - p_{\mathrm{k}}) q_{\mathrm{j}} + \int_{\Omega_{\mathrm{el}}} \beta_{\mathrm{j}}^{\mathrm{e}} p_{\mathrm{j}} q_{\mathrm{j}}, \tag{7e}$$

$$\mathcal{F}_{\mathrm{j}}(q_{\mathrm{j}}) = \int_{\Omega_{\mathrm{el}}} g_{\mathrm{j}} q_{\mathrm{j}}, \tag{7f}$$

$$\mathcal{A}_{\mathrm{f}}(\boldsymbol{u}, \boldsymbol{v}) = \int_{\Omega_{\mathrm{f}}} \sigma_{\mathrm{f}}(\boldsymbol{u}) : \varepsilon_h(\boldsymbol{v}) - \sum_{F \in \mathscr{F}_{\mathrm{f}}^{\mathrm{I}} \cup \mathscr{F}_{\mathrm{f}}^{\mathrm{D}}} \int_F \left(\{\!\{ \sigma_{\mathrm{f}}(\boldsymbol{u}) \}\!\} : [\![\boldsymbol{v}]\!] + [\![\boldsymbol{u}]\!] : \{\!\{ \sigma_{\mathrm{f}}(\boldsymbol{v}) \}\!\} - \gamma_{\boldsymbol{v}} [\![\boldsymbol{u}]\!] : [\![\boldsymbol{v}]\!] \right), \tag{7g}$$

$$\mathcal{B}_{\mathrm{f}}(p, \boldsymbol{v}) = -\int_{\Omega_{\mathrm{f}}} p \operatorname{div}_h \boldsymbol{v} + \sum_{F \in \mathscr{F}_{\mathrm{f}}^{\mathrm{I}} \cup \mathscr{F}_{\mathrm{f}}^{\mathrm{D}}} \int_F \{\!\{ p I \}\!\} : [\![\boldsymbol{v}]\!], \tag{7h}$$

$$\mathcal{F}_{\mathrm{f}}(\boldsymbol{v}) = \int_{\Omega_{\mathrm{f}}} \boldsymbol{f}_{\mathrm{f}} \cdot \boldsymbol{v}, \tag{7i}$$

$$\mathcal{S}(p, q) = \sum_{F \in \mathscr{F}_{\mathrm{f}}^{\mathrm{I}}} \int_F \gamma_p [\![p]\!] \cdot [\![q]\!], \tag{7j}$$

$$\mathcal{J}(p_{\mathrm{E}}, \boldsymbol{w}, \boldsymbol{v}) = \sum_{F \in \mathscr{F}^{\Sigma}} \int_F \left(\{\!\{ p_{\mathrm{E}} I \}\!\} : [\![\boldsymbol{w}, \boldsymbol{v}]\!] \right), \tag{7k}$$

where $\nabla_h, \varepsilon_h, \operatorname{div}_h$ denote the element-wise gradient, symmetric gradient, and divergence operators, respectively, and the stress tensors $\sigma_{\mathrm{el}}, \sigma_{\mathrm{f}}$ are implicitly defined in terms of these piecewise operators. The parameters $\eta, \zeta_{\mathrm{j}}, \gamma_{\boldsymbol{v}}, \gamma_p$ appearing in these forms are defined as follows [38,40]:

$$\eta = \overline{\eta} \frac{\overline{\mathbb{C}}_{\mathrm{el}}^K}{\{h\}_{\mathrm{H}}}, \qquad \zeta_{\mathrm{j}} = \overline{\zeta}_{\mathrm{j}} \frac{\overline{k}_{\mathrm{j}}^K}{\sqrt{\mu_{\mathrm{j}}} \{h\}_{\mathrm{H}}}, \qquad \gamma_{\boldsymbol{v}} = \overline{\gamma}_{\boldsymbol{v}} \frac{\mu}{\{h\}_{\mathrm{H}}}, \qquad \gamma_p = \overline{\gamma}_p \{h\}_{\mathrm{H}}, \tag{8}$$

where $\{h\}_{\mathrm{H}}$ denotes the harmonic average on $K^{\pm}$ (with $\{h\}_{\mathrm{H}} = h_K$ on Dirichlet faces) $\overline{\mathbb{C}}_{\mathrm{el}}^K = \|\mathbb{C}_{\mathrm{el}}^{1/2}|_K\|_2^2, \overline{k}_{\mathrm{j}}^K = \|K_{\mathrm{j}}^{1/2}|_K\|_2^2$ are the L^2-norms of the symmetric second-order tensors appearing in the elasticity and Darcy equations, for each $K \in \mathscr{T}_{\mathrm{el}}$, and $\overline{\eta}, \overline{\zeta}_{\mathrm{j}} \, \forall \mathrm{j} \in J, \overline{\gamma}_{\boldsymbol{v}}, \overline{\gamma}_p$ are penalty constants to be chosen large enough.

The form $J(\cdot, \cdot, \cdot)$ is the piecewise discontinuous version of the interface form $\mathfrak{J}(\cdot, \cdot, \cdot)$ derived in Remark 1. Indeed, for any $p_{\mathrm{E}} \in H^1(\mathscr{T}_{h_{\mathrm{el}}}), \boldsymbol{w} \in [H^1(\mathscr{T}_{h,\mathrm{el}})]^d, \boldsymbol{v} \in [H^1(\mathscr{T}_{h,\mathrm{f}})]^d$,

$$\mathfrak{J}(q_{\mathrm{E}}, \boldsymbol{w}, \boldsymbol{v}) = \sum_{F \in \mathscr{F}^{\Sigma}} \int_F \left[p_{\mathrm{E}} I : (\boldsymbol{w} \odot \boldsymbol{n}_{\mathrm{el}} + \boldsymbol{v} \odot \boldsymbol{n}_{\mathrm{f}}) - q_{\mathrm{E}} I : (\partial_t \boldsymbol{d} \odot \boldsymbol{n}_{\mathrm{el}} + \boldsymbol{u} \odot \boldsymbol{n}_{\mathrm{f}}) \right]$$

$$= \sum_{F \in \mathscr{F}^{\Sigma}} \int_F \left[\{\!\{ p_{\mathrm{E}} I \}\!\} : [\![\boldsymbol{w}, \boldsymbol{v}]\!] - [\![\partial_t \boldsymbol{d}, \boldsymbol{u}]\!] : \{\!\{ q_{\mathrm{E}} I \}\!\} \right], \tag{9}$$

where we have used the identity $\boldsymbol{a} \cdot \boldsymbol{b} = \boldsymbol{a} \odot \boldsymbol{b} : I, \forall \boldsymbol{a}, \boldsymbol{b} \in \mathbb{R}^d$ and then the definition of the average and jump operators introduced in Section 3.1.

Finally, the semidiscrete formulation reads as follows:

For any $t \in (0, T]$, find $(\boldsymbol{d}_h, \{p_{\mathrm{j},h}\}_{\mathrm{j} \in J}, \boldsymbol{u}_h, p_h) \in \boldsymbol{W}_h^{\mathrm{DG}} \times \left(\times_{\mathrm{j} \in J} Q_{\mathrm{j},h}^{\mathrm{DG}} \right) \times \boldsymbol{V}_h^{\mathrm{DG}} \times Q_h^{\mathrm{DG}}$ such that

$$
\begin{aligned}
&(\rho_{\mathrm{el}}\partial_{tt}^2 \boldsymbol{d}_h, \boldsymbol{w}_h)_{\Omega_{\mathrm{el}}} + \mathcal{L}_{\mathrm{el}}(\boldsymbol{d}_h, \{p_{k,h}\}_{k\in J}; \boldsymbol{w}_h) - \mathcal{F}_{\mathrm{el}}(\boldsymbol{w}_h) \\
&\quad + \sum_{\mathrm{j}\in J}\left[(c_{\mathrm{j}}\partial_t p_{\mathrm{j},h}, q_{\mathrm{j},h})_{\Omega_{\mathrm{el}}} + \mathcal{L}_{\mathrm{j}}(\{p_{k,h}\}_{k\in J}, \partial_t \boldsymbol{d}_h; q_{\mathrm{j},h}) - \mathcal{F}_{\mathrm{j}}(q_{\mathrm{j},h}) \right] \\
&\quad + (\rho_{\mathrm{f}}\partial_t \boldsymbol{u}_h, \boldsymbol{v}_h)_{\Omega_{\mathrm{f}}} + \mathcal{L}_{\mathrm{f}}(\boldsymbol{u}_h, p_h; \boldsymbol{v}_h, q_h) - \mathcal{F}_{\mathrm{f}}(\boldsymbol{v}_h) \\
&\quad + \mathcal{J}(p_{\mathrm{E},h}, \boldsymbol{w}_h, \boldsymbol{v}_h) - \mathcal{J}(q_{\mathrm{E},h}, \partial_t \boldsymbol{d}_h, \boldsymbol{u}_h) = 0 \\
&\forall \boldsymbol{w}_h \in \boldsymbol{W}_h^{\mathrm{DG}}, \boldsymbol{v}_h \in \boldsymbol{V}_h^{\mathrm{DG}}, q_h \in Q_h^{\mathrm{DG}}, q_{\mathrm{j},h} \in Q_{\mathrm{j},h}^{\mathrm{DG}}.
\end{aligned}
\tag{10}
$$

Problem (10) is supplemented with suitable initial conditions $\boldsymbol{d}_h(0), \dot{\boldsymbol{d}}_h(0), \{p_{\mathrm{j},h}(0)\}_{\mathrm{j}\in J}, \boldsymbol{u}_h(0)$ that are projections of the initial data introduced in (1) onto the corresponding DG spaces. The bilinear forms appearing in (10) are defined as

$$
\mathcal{L}_{\mathrm{el}}(\boldsymbol{d}, \{p_k\}_{k\in J}; \boldsymbol{w}) = \mathcal{A}_{\mathrm{el}}(\boldsymbol{d}, \boldsymbol{w}) + \sum_{k\in J} \mathcal{B}_k(p_k, \boldsymbol{w}),
\tag{11a}
$$

$$
\mathcal{L}_{\mathrm{j}}(\{p_k\}_{k\in J}, \partial_t \boldsymbol{d}; q_{\mathrm{j}}) = \mathcal{A}_{\mathrm{j}}(p_{\mathrm{j}}, q_{\mathrm{j}}) + C_{\mathrm{j}}(\{p_k\}_{k\in J}, q_{\mathrm{j}}) - \mathcal{B}_{\mathrm{j}}(q_{\mathrm{j}}, \partial_t \boldsymbol{d}), \qquad \forall \mathrm{j} \in J,
\tag{11b}
$$

$$
\mathcal{L}_{\mathrm{f}}(\boldsymbol{u}, p; \boldsymbol{v}, q) = \mathcal{A}_{\mathrm{f}}(\boldsymbol{u}, \boldsymbol{v}) + \mathcal{B}_{\mathrm{f}}(p, \boldsymbol{v}) - \mathcal{B}_{\mathrm{f}}(q, \boldsymbol{u}) + S(p, q).
\tag{11c}
$$

3.3. Algebraic formulation

We introduce suitable sets of basis functions such that $\operatorname{span}\{\boldsymbol{\varphi}_{\mathrm{el}}^i\}_{i=0}^{N_{\mathrm{el}}} = \boldsymbol{W}_h^{\mathrm{DG}}$, $\operatorname{span}\{\boldsymbol{\varphi}_{\mathrm{el}}^i\}_{i=0}^{N_{\mathrm{f}}} = \boldsymbol{V}_h^{\mathrm{DG}}$, $\operatorname{span}\{\psi^i\}_{i=0}^{N_p} = Q_h^{\mathrm{DG}}$, $\operatorname{span}\{\psi_{\mathrm{j}}^i\}_{i=0}^{N_{\mathrm{j}}} = Q_{\mathrm{j},h}^{\mathrm{DG}}$ for $\mathrm{j}\in J$. Denoting by uppercase letters the d.o.f. vectors corresponding to the problem unknowns, the (formal) algebraic form of (10) is the following:
Given $\boldsymbol{D}_0, \dot{\boldsymbol{D}}_0, \boldsymbol{U}_0, \boldsymbol{P}_{\mathrm{j}0}, \mathrm{j}\in J$, find $\boldsymbol{D}, \boldsymbol{U}, \boldsymbol{P}, \boldsymbol{P}_{\mathrm{j}}, \mathrm{j}\in J$ such that

$$
\begin{bmatrix}
M_{\mathrm{el}}\partial_{tt}^2 + A_{\mathrm{el}} & B_A^T & \cdots & B_E^T + J_{\mathrm{el}}^T & 0 & 0 \\
-B_A \partial_t & M_A \partial_t + A_A + C_{AA} & \cdots & C_{AE} & 0 & 0 \\
\vdots & \vdots & \vdots & \vdots & \vdots & \vdots \\
-(B_E + J_{\mathrm{el}})\partial_t & C_{EA} & \cdots & M_E \partial_t + A_E + C_{EE} & -J_{\mathrm{f}} & 0 \\
0 & 0 & \cdots & J_{\mathrm{f}}^T & M_{\mathrm{f}}\partial_t + A_{\mathrm{f}} & B_{\mathrm{f}}^T \\
0 & 0 & \cdots & 0 & -B_{\mathrm{f}} & S
\end{bmatrix}
\begin{bmatrix}
\boldsymbol{D} \\ \boldsymbol{P}_A \\ \vdots \\ \boldsymbol{P}_E \\ \boldsymbol{U} \\ \boldsymbol{P}
\end{bmatrix}
=
\begin{bmatrix}
\boldsymbol{F}_{\mathrm{el}} \\ \boldsymbol{F}_A \\ \vdots \\ \boldsymbol{F}_E \\ \boldsymbol{F}_{\mathrm{f}} \\ \boldsymbol{0}
\end{bmatrix}
$$

The matrices and vectors of this formulation are defined as follows (where $\star = \mathrm{el}, \mathrm{f}$):

$$
\begin{aligned}
&[M_\star]_{ij} = (\rho_\star \boldsymbol{\varphi}_\star^j, \boldsymbol{\varphi}_\star^i)_{\Omega_\star}, && [M_{\mathrm{j}}]_{ij} = (c_{\mathrm{j}}\psi_{\mathrm{j}}^j, \phi_{\mathrm{j}}^i)_{\Omega_{\mathrm{el}}}, && [S]_{ij} = S(\psi^j, \phi^i) \\
&[A_\star]_{ij} = \mathcal{A}_\star(\boldsymbol{\varphi}_\star^j, \boldsymbol{\varphi}_\star^i), && [A_{\mathrm{j}}]_{ij} = \mathcal{A}_{\mathrm{j}}(\psi_{\mathrm{j}}^j, \phi_{\mathrm{j}}^i), && [C_{\mathrm{j}}]_{ij} = C_{\mathrm{j}}(\{\psi_k^j\}_{k\in J}, \psi_{\mathrm{j}}^i), \\
&[B_{\mathrm{f}}]_{ij} = \mathcal{B}_{\mathrm{f}}(\psi^i, \boldsymbol{\varphi}_{\mathrm{f}}^j), && [B_{\mathrm{j}}]_{ij} = \mathcal{B}_{\mathrm{j}}(\psi_{\mathrm{j}}^i, \boldsymbol{\varphi}_{\mathrm{el}}^i), && [J_\star]_{ij} = \sum_{F\in\mathscr{F}^\Sigma} \int_F \{\!\{q_E^j I\}\!\} : \boldsymbol{\varphi}_\star^i \odot \boldsymbol{n}_\star, \\
&[F_\star]_i = \mathcal{F}_\star(\boldsymbol{\varphi}_\star^i), && [F_{\mathrm{j}}]_i = \mathcal{F}_{\mathrm{j}}(\psi_{\mathrm{j}}^i).
\end{aligned}
$$

4. A priori analysis of the semidiscrete problem

For the analysis contained in this section, we consider a generic set J of $N_J \in \mathbb{N}_0$ compartments and we assume that all the physical parameters of the model (defined in Table 1) are piecewise constant. For $r \geq 1$, we introduce the following broken norms [38,40]:

$$
\|\boldsymbol{d}\|_{\mathrm{DG,D}}^2 = \|\mathbb{C}_{\mathrm{el}}^{\frac{1}{2}} 2[\varepsilon_h(\boldsymbol{d})]\|_{L^2(\mathscr{T}_{\mathrm{el}})}^2 + \|\sqrt{\eta}[\![\boldsymbol{d}]\!]\|_{\mathscr{F}_{\mathrm{el},h}^{\mathrm{I}} \cup \mathscr{F}_{\mathrm{el},h}^{\mathrm{D}}}^2 \qquad \forall \boldsymbol{d} \in \boldsymbol{H}^r(\mathscr{T}_h),
\tag{12a}
$$

$$
\|p\|_{\mathrm{DG,P_j}}^2 = \|\mu_{\mathrm{j}}^{-1/2} K_{\mathrm{j}}^{1/2} \nabla_h p\|_{L^2(\mathscr{T}_{\mathrm{el}})}^2 + \|\sqrt{\zeta_{\mathrm{j}}}[\![p]\!]\|_{\mathscr{F}_{\mathrm{el},h}^{\mathrm{I}} \cup \mathscr{F}_{\mathrm{el},h}^{\mathrm{D_j}}}^2 \qquad \forall p \in H^r(\mathscr{T}_h),
\tag{12b}
$$

$$
\|\boldsymbol{u}\|_{\mathrm{DG,U}}^2 = \|\sqrt{2\mu}\,\varepsilon_h(\boldsymbol{u})\|_{L^2(\mathscr{T}_{\mathrm{f}})}^2 + \|\sqrt{\gamma_v}[\![\boldsymbol{u}]\!]\|_{\mathscr{F}_{\mathrm{f},h}^{\mathrm{I}}}^2 \qquad \forall \boldsymbol{u} \in \boldsymbol{H}^r(\mathscr{T}_h),
\tag{12c}
$$

$$
\|q\|_{\mathrm{DG,P_f}}^2 = \|q\|_{L^2(\Omega_{\mathrm{f}})}^2 + \|\sqrt{\gamma_p}[\![q]\!]\|_{\mathscr{F}_{\mathrm{f},h}^{\mathrm{I}} \cup \mathscr{F}_{\mathrm{f},h}^{\mathrm{D}}}^2 \qquad \forall q \in H^r(\mathscr{T}_h).
\tag{12d}
$$

We introduce the energy norms at time $t \in (0, T]$

$$
\|(\boldsymbol{d}, \{p_{\mathrm{j}}\}_{\mathrm{j}\in J})\|_{\mathrm{el},t} = \left[\|\sqrt{\rho_{\mathrm{el}}}\partial_t \boldsymbol{d}(t)\|_{\Omega_{\mathrm{el}}}^2 + \|\boldsymbol{d}(t)\|_{\mathrm{DG,D}}^2 \right.
$$

$$+ \sum_{j \in J} \left(\| \sqrt{c_j} p_j(t) \|_{\Omega_{el}}^2 + \int_0^t \left(\| p_j(s) \|_{DG,P_j}^2 + \| \sqrt{\beta_j^e} p_j(s) \|_{\Omega_{el}}^2 \right) ds \right) \Bigg]^{1/2} ,$$

$$\| (\boldsymbol{u}, p) \|_{f,t} = \left[\| \sqrt{\rho_f} \boldsymbol{u}(t) \|_{\Omega_f}^2 + \int_0^t \left(\| \boldsymbol{u}(s) \|_{DG,U}^2 + \| p(s) \|_{DG,P_f}^2 \right) ds \right]^{1/2} ,$$

and set

$$\| (\boldsymbol{d}, \{ p_j \}_{j \in J}, \boldsymbol{u}, p) \|_{EN,t} = \left[\| (\boldsymbol{d}, \{ p_j \}_{j \in J}) \|_{el,t}^2 + \| (\boldsymbol{u}, p) \|_{f,t}^2 \right]^{1/2} . \tag{13}$$

For the sake of simplicity, in the inequalities appearing in the following analysis, we neglect the dependencies on the model parameters and the polynomial degree m, and we use the notation $x \lesssim y$ to indicate that $\exists C > 0 : x \leq C y$, where C is independent of the mesh discretization parameters. Moreover, we make the following assumption on the mesh [25,26]:

Assumption 1. For each $h > 0$, the two meshes $\mathscr{T}_{h,el}, \mathscr{T}_{h,f}$ are aligned with Σ, namely there is no gap nor overlap between them (hanging nodes are allowed). Moreover, denoting by $\mathscr{T}_h$ the union of $\mathscr{T}_{h,el}$ and $\mathscr{T}_{h,f}$, we consider a sequence of meshes $\{ \mathscr{T}_h \}_{h>0}$ satisfying the regularity requirements of [38]:

- $\{ \mathscr{T}_h \}_{h>0}$ is h-uniformly polytopic-regular, namely for each $K \in \mathscr{T}_h$ there exists a set $\{ S_K^F \}_{F \subset \partial K}$ of non-overlapping d-dimensional simplices contained in $\overline{K}$ such that

$$\forall F \subset \partial K : \ \overline{F} = \overline{\partial K} \cap \overline{S_K^F} \text{ it holds that } h_K \lesssim d |S_K^F| |F|^{-1} ,$$

  where h_K is the diameter of K, and the cardinality of $\{ S_K^F \}_{F \subset \partial K}$ does not depend on $h > 0$.
- There exists a shape-regular simplicial covering $\widehat{\mathscr{T}}_h$ of $\mathscr{T}_h$ such that, for each $K \in \mathscr{T}_h, \widehat{K} \in \widehat{\mathscr{T}}_h$ with $\widehat{K} \subseteq K$,

$$h_K \lesssim h_{\widehat{K}}, \max_{K \in \mathscr{T}_h} \mathrm{card} \{ K' \in \mathscr{T}_h : \exists \widehat{K} \in \widehat{\mathscr{T}}_h \text{ such that } K \subset \widehat{K} \text{ and } K' \cap \widehat{K} \neq \emptyset \} \lesssim 1 .$$

- The mesh size satisfies a local bounded variation property:

$$\forall K_1, K_2 \in \mathscr{T}_h : \ |\partial K_1 \cap \partial K_2|_{d-1} > 0 \qquad h_{K_1} \lesssim h_{K_2} \lesssim h_{K_1} ,$$

  with $| \cdot |_{d-1}$ denotes the $(d-1)$-dimensional measure and all the hidden constants independent of h and the number of faces of K_1 and K_2.

Under these assumptions, we can prove the following stability result:

Theorem 1 (Stability estimate). *Let Assumption 1 hold true and let us also assume that the penalty constants defined in (8) are chosen sufficiently large. Then, the semidiscrete solution* $(\boldsymbol{d}_h, \{ p_{j,h} \}_{j \in J}, \boldsymbol{u}_h, p_h)$ *of* (10) *satisfies the following inequality for each* $t \in (0, T]$:

$$\| (\boldsymbol{d}_h, \{ p_{j,h} \}_{j \in J}, \boldsymbol{u}_h, p_h) \|_{EN,t} \lesssim \| (\boldsymbol{d}_h, \{ p_{j,h} \}_{j \in J}, \boldsymbol{u}_h, 0) \|_{EN,0}$$
$$+ \int_0^t \left(\frac{1}{\sqrt{\rho_{el}}} \| \boldsymbol{f}_{el} \|_{\Omega_{el}} + \sum_{j \in J} \frac{1}{\sqrt{c_j}} \| g_j \|_{\Omega_{el}} + \frac{1}{\sqrt{\rho_f}} \| \boldsymbol{f}_f \|_{\Omega_f} \right) ds , \tag{14}$$

where, according to the initial conditions of (1),

$$\| (\boldsymbol{d}_h, \{ p_{j,h} \}_{j \in J}, \boldsymbol{u}_h, 0) \|_{EN,0} = \left[\| \sqrt{\rho_{el}} \dot{\boldsymbol{d}}_h^0 \|_{\Omega_{el}}^2 + \| \boldsymbol{d}_h^0 \|_{DG,D}^2 + \sum_{j \in J} \| \sqrt{c_j} p_{j,h}^0 \|_{\Omega_{el}}^2 + \| \sqrt{\rho_f} \boldsymbol{u}_h^0 \|_{\Omega_f}^2 \right]^{1/2} .$$

Proof. Let us fix a time $t \in (0, T]$ and consider the following test functions in (6): $\boldsymbol{w} = \partial_t \boldsymbol{d}(t), \boldsymbol{v} = \boldsymbol{u}(t), q = p(t), q_j = p_j(t) \ \forall j \in J$. With this choice of test functions, the terms $\mathcal{J}$ cancel out, as well as the $\mathcal{B}$ forms in the $\mathcal{L}$ terms.[1] Therefore, (6) becomes

---

[1] In the next steps, although the $\mathcal{B}_f$ terms cancel out due to the choice of test functions, we keep writing the complete form $\mathcal{L}_f$ to facilitate the application of a generalized inf-sup condition (see Appendix A, Theorem 5).

$$(\rho_{\mathrm{el}}\partial_{tt}^2\boldsymbol{d}(t),\partial_t\boldsymbol{d}(t))_{\Omega_{\mathrm{el}}} + \mathcal{A}_{\mathrm{el}}(\boldsymbol{d}(t),\partial_t\boldsymbol{d}(t))$$
$$+ \sum_{j\in J}\left[(c_j\partial_t p_j(t),p_j(t))_{\Omega_{\mathrm{el}}} + \mathcal{A}_j(p_j(t),p_j(t)) + C_j(\{p_k(t)\}_{k\in J},p_j(t))\right]$$
$$+ (\rho_{\mathrm{f}}\partial_t\boldsymbol{u}(t),\boldsymbol{u}(t))_{\Omega_{\mathrm{f}}} + \mathcal{L}_{\mathrm{f}}(\boldsymbol{u}(t),p(t);\boldsymbol{u}(t),p(t)) \tag{15}$$
$$= \mathcal{F}_{\mathrm{el}}(\partial_t\boldsymbol{d}(t)) + \sum_{j\in J}\mathcal{F}_j(p_j(t)) + \mathcal{F}_{\mathrm{f}}(\boldsymbol{u}(t)).$$

Proceeding as in [38], we integrate (15) w.r.t. time and we can employ integration by parts in time in the following terms to obtain

$$\int_0^t (\rho_{\mathrm{el}}\partial_{tt}^2\boldsymbol{d}(s),\partial_t\boldsymbol{d}(s))_{\Omega_{\mathrm{el}}}ds = \frac{1}{2}\|\sqrt{\rho_{\mathrm{el}}}\partial_t\boldsymbol{d}(t)\|_{\Omega_{\mathrm{el}}}^2 - \frac{1}{2}\|\sqrt{\rho_{\mathrm{el}}}\dot{\boldsymbol{d}}^0\|_{\Omega_{\mathrm{el}}}^2,$$

$$\int_0^t \mathcal{A}_{\mathrm{el}}(\boldsymbol{d}(s),\partial_t\boldsymbol{d}(s))ds = \frac{1}{2}\mathcal{A}_{\mathrm{el}}(\boldsymbol{d}(t),\boldsymbol{d}(t)) - \frac{1}{2}\mathcal{A}_{\mathrm{el}}(\boldsymbol{d}^0,\boldsymbol{d}^0)$$

$$\int_0^t (c_j\partial_t p_j(s),p_j(s))_{\Omega_{\mathrm{el}}}ds = \frac{1}{2}\|\sqrt{c_j}p_j(t)\|_{\Omega_{\mathrm{el}}}^2 - \frac{1}{2}\|\sqrt{c_j}p_j^0\|_{\Omega_{\mathrm{el}}}^2, \qquad \forall j\in J,$$

$$\int_0^t (\rho_{\mathrm{f}}\partial_t\boldsymbol{u}(s),\boldsymbol{u}(s))_{\Omega_{\mathrm{f}}}ds = \frac{1}{2}\|\sqrt{\rho_{\mathrm{f}}}\boldsymbol{u}(t)\|_{\Omega_{\mathrm{f}}}^2 - \frac{1}{2}\|\sqrt{\rho_{\mathrm{f}}}\boldsymbol{u}^0\|_{\Omega_{\mathrm{f}}}^2.$$

Using these identities and the definition of the bulk and broken norms introduced above, we can rewrite the left-hand side of (15) (integrated over time) as follows, and use Cauchy-Schwarz's and Young's inequalities on the right-hand side:

$$\|\sqrt{\rho_{\mathrm{el}}}\partial_t\boldsymbol{d}(t)\|_{\Omega_{\mathrm{el}}}^2 \|\sqrt{\rho_{\mathrm{el}}}\dot{\boldsymbol{d}}^0\|_{\Omega_{\mathrm{el}}}^2 + \mathcal{A}_{\mathrm{el}}(\boldsymbol{d}(t),\boldsymbol{d}(t)) - \mathcal{A}_{\mathrm{el}}(\boldsymbol{d}^0,\boldsymbol{d}^0)$$
$$+ \sum_{j\in J}\left[\|\sqrt{c_j}p_j(t)\|_{\Omega_{\mathrm{el}}}^2 - \|\sqrt{c_j}p_j^0\|_{\Omega_{\mathrm{el}}}^2 + 2\int_0^t \left(\mathcal{A}_j(p_j(s),p_j(s)) + C_j(\{p_k(s)\}_{k\in J},p_j(s))\right)ds\right]$$
$$+ \|\sqrt{\rho_{\mathrm{f}}}\boldsymbol{u}(t)\|_{\Omega_{\mathrm{f}}}^2 - \|\sqrt{\rho_{\mathrm{f}}}\boldsymbol{u}^0\|_{\Omega_{\mathrm{f}}}^2 + 2\int_0^t \mathcal{L}_{\mathrm{f}}(\boldsymbol{u}(s),p(s);\boldsymbol{u}(s),p(s))ds \tag{16}$$
$$\leq \int_0^t \left(\left\|\frac{1}{\sqrt{\rho_{\mathrm{el}}}}\boldsymbol{f}_{\mathrm{el}}(s)\right\|_{\Omega_{\mathrm{el}}}^2 + \|\sqrt{\rho_{\mathrm{el}}}\partial_t\boldsymbol{d}(s)\|_{\Omega_{\mathrm{el}}}^2 + \sum_{j\in J}\left\|\frac{1}{\sqrt{c_j}}g_j(s)\right\|_{\Omega_{\mathrm{el}}}^2\right.$$
$$\left.+ \sum_{j\in J}\|\sqrt{c_j}p_j(s)\|_{\Omega_{\mathrm{el}}}^2 + \left\|\frac{1}{\sqrt{\rho_{\mathrm{f}}}}\boldsymbol{f}_{\mathrm{f}}(s)\right\|_{\Omega_{\mathrm{f}}}^2 + \|\sqrt{\rho_{\mathrm{f}}}\boldsymbol{u}(s)\|_{\Omega_{\mathrm{f}}}^2\right)ds.$$

We now consider continuity and coercivity results for the bilinear forms appearing in (16) with respect to the broken norms (12). These results, proven in [38,40], are reported in Appendix A (Theorem 5) and they include an inf-sup condition for the form $\mathcal{B}_{\mathrm{f}}$, with a constant $\beta_{\mathrm{f},h}$ independent of the mesh elements size. According to [40], if γ_v is large enough, there exists $\alpha > 0$ such that $\alpha = \mathcal{O}(\beta_{\mathrm{f},h}^{-2})$ and

$$\mathcal{L}_{\mathrm{f}}(\boldsymbol{u}(s),p(s);\boldsymbol{u}(s),p(s)) \geq \alpha(\|\boldsymbol{u}(s)\|_{\mathrm{DG,U}}^2 + \|p(s)\|_{\mathrm{DG,P_f}}^2).$$

Analogously, the coercivity results of the forms $\mathcal{A}_{\mathrm{el}},\mathcal{A}_j,C_j$ and the continuity of $\mathcal{A}_{\mathrm{el}}$ yield [38]

$$\mathcal{A}_{\mathrm{el}}(\boldsymbol{d}(t),\boldsymbol{d}(t)) - \mathcal{A}_{\mathrm{el}}(\boldsymbol{d}^0,\boldsymbol{d}^0) + 2\sum_{j\in J}\int_0^t \left(\mathcal{A}_j(p_j(s),p_j(s)) + C_j(\{p_k(s)\}_{k\in J},p_j(s))\right)ds$$

$$\gtrsim \|\boldsymbol{d}(t)\|_{\mathrm{DG,D}}^2 - \|\boldsymbol{d}^0\|_{\mathrm{DG,D}}^2 + \sum_{j\in J}\int_0^t \left(\|p_j(s)\|_{\mathrm{DG,P_j}}^2 + \|\sqrt{\beta_j^{\mathrm{e}}}p_j(s)\|_{\Omega_{\mathrm{el}}}^2\right)ds.$$

We can use these results on the left-hand side of (16) to obtain

$$\| \sqrt{\rho_{\mathrm{el}}} \partial_t \boldsymbol{d}(t) \|_{\Omega_{\mathrm{el}}}^2 + \| \boldsymbol{d}(t) \|_{\mathrm{DG,D}}^2 + \sum_{\mathrm{j} \in J} \left[\| \sqrt{c_{\mathrm{j}}} p_{\mathrm{j}}(t) \|_{\Omega_{\mathrm{el}}}^2 + \int_0^t \left(\| p_{\mathrm{j}}(s) \|_{\mathrm{DG,P_j}}^2 + \| \sqrt{\beta_{\mathrm{j}}^{\mathrm{e}}} p_{\mathrm{j}}(s) \|_{\Omega_{\mathrm{el}}}^2 \right) ds \right]$$

$$- \| \sqrt{\rho_{\mathrm{el}}} \dot{\boldsymbol{d}}^0 \|_{\Omega_{\mathrm{el}}}^2 - \| \boldsymbol{d}^0 \|_{\mathrm{DG,D}}^2 - \sum_{\mathrm{j} \in J} \| \sqrt{c_{\mathrm{j}}} p_{\mathrm{j}}^0 \|_{\Omega_{\mathrm{el}}}^2$$

$$+ \| (\boldsymbol{u}(t), p(t)) \|_{\mathrm{f},t}^2 - \| \sqrt{\rho_{\mathrm{f}}} \boldsymbol{u}^0 \|_{\Omega_{\mathrm{f}}}^2$$

$$\lesssim \int_0^t \left(\left\| \frac{1}{\sqrt{\rho_{\mathrm{el}}}} \boldsymbol{f}_{\mathrm{el}}(s) \right\|_{\Omega_{\mathrm{el}}}^2 + \sum_{\mathrm{j} \in J} \left\| \frac{1}{\sqrt{c_{\mathrm{j}}}} g_{\mathrm{j}}(s) \right\|_{\Omega_{\mathrm{el}}}^2 + \left\| \frac{1}{\sqrt{\rho_{\mathrm{f}}}} \boldsymbol{f}_{\mathrm{f}}(s) \right\|_{\Omega_{\mathrm{f}}}^2 \right) ds.$$

The definitions of $\| \cdot \|_{\mathrm{EN},t}$ and $\| \cdot \|_{\mathrm{EN},0}$ and the fact that $\rho_{\mathrm{el}}, c_{\mathrm{j}}, \rho_{\mathrm{f}}$ are constant conclude the proof. $\quad\square$

We now proceed to derive an a-priori error estimate for the error introduced by the space discretization of the problem. For any $t \in (0, T]$, let $(\boldsymbol{d}, \{p_{\mathrm{j}}\}_{\mathrm{j} \in J}, \boldsymbol{u}, p)$ denote the weak solution of problem (6) and let $(\boldsymbol{d}_h, \{p_{\mathrm{j},h}\}_{\mathrm{j} \in J}, \boldsymbol{u}_h, p_h)$ denote the semidiscrete solution of problem (10), obtained with sufficiently large stability parameters as defined in (8).

Using the inverse trace inequality [25,48]

$$\| \phi \|_{\partial K}^2 \lesssim h_K^{-1} \| \phi \|_K^2 \qquad \forall \phi \in \mathbb{P}^m(K), K \in \mathscr{T}_h, \tag{17}$$

we can state the following continuity result for the interface forms, whose proof is provided in Appendix B:

Lemma 2. *Under Assumption 1, the following inequalities hold:*

$$|\mathcal{J}(q, \boldsymbol{w}_h, \boldsymbol{v}_h)| \lesssim \| \eta^{1/2} q \|_{\mathscr{F}_h^\Sigma} \| \boldsymbol{w}_h \|_{\mathrm{DG,D}} + \| \gamma_p^{-1/2} q \|_{\mathscr{F}_h^\Sigma} \| \boldsymbol{v}_h \|_{\mathrm{DG,U}}$$
$$\forall q \in H^2(\mathscr{T}_{h,\mathrm{el}}), \boldsymbol{w}_h \in \boldsymbol{W}_h^{\mathrm{DG}}, \boldsymbol{v}_h \in \boldsymbol{V}_h^{\mathrm{DG}},$$

$$|\mathcal{J}(q_h, \boldsymbol{w}, \boldsymbol{v})| \lesssim \| q_h \|_{\mathrm{DG,P_f}} \| \eta^{1/2} \boldsymbol{w} \|_{\mathscr{F}_h^\Sigma} + \| q_h \|_{\mathrm{DG,P_f}} \| \gamma_{\boldsymbol{v}}^{1/2} \boldsymbol{v} \|_{\mathscr{F}_h^\Sigma}$$
$$\forall q_h \in Q_{\mathrm{E},h}^{\mathrm{DG}}, \boldsymbol{w} \in [H^2(\mathscr{T}_{h,\mathrm{f}})]^d, \boldsymbol{v} \in [H^2(\mathscr{T}_{h,\mathrm{f}})]^d.$$

We introduce the following additional norms for non-discrete functions:

$$\|\|\boldsymbol{w}\|\|_{\mathrm{D}}^2 = \| \boldsymbol{w} \|_{\mathrm{DG,D}}^2 + \| \eta^{-1/2} \{\!\!\{ \sigma_{\mathrm{el}}(\boldsymbol{w}) \}\!\!\} \|_{\mathscr{F}_{\mathrm{el},h}^{\mathrm{I}} \cup \mathscr{F}_{\mathrm{el},h}^{\mathrm{D}}}^2 \qquad\qquad \forall \boldsymbol{w} \in [H^2(\mathscr{T}_{h,\mathrm{el}})]^d,$$

$$\|\|q_{\mathrm{j}}\|\|_{\mathrm{P_j}}^2 = \| q_{\mathrm{j}} \|_{\mathrm{DG,P_j}}^2 + \| \zeta^{-1/2} \{\!\!\{ \frac{1}{\mu_{\mathrm{j}}} K_{\mathrm{j}} \nabla_h q_{\mathrm{j}} \}\!\!\} \|_{\mathscr{F}_{\mathrm{el},h}^{\mathrm{I}} \cup \mathscr{F}_{\mathrm{el},h}^{\mathrm{D_j}}}^2 \qquad\qquad \forall q_{\mathrm{j}} \in H^2(\mathscr{T}_{h,\mathrm{el}}), \qquad \forall \mathrm{j} \in J,$$

$$\|\|\boldsymbol{v}\|\|_{\mathrm{U}}^2 = \| \boldsymbol{v} \|_{\mathrm{DG,U}}^2 + \| \gamma_{\boldsymbol{v}}^{-1/2} \{\!\!\{ \sigma_{\mathrm{f}}(\boldsymbol{v}) \}\!\!\} \|_{\mathscr{F}_{\mathrm{f},h}^{\mathrm{I}} \cup \mathscr{F}_{\mathrm{f},h}^{\mathrm{D}}}^2 \qquad\qquad \forall \boldsymbol{v} \in [H^2(\mathscr{T}_{h,\mathrm{f}})]^d,$$

$$\|\|q\|\|_{\mathrm{P_f}}^2 = \| q \|_{\mathrm{DG,P_f}}^2 + \| \gamma_p^{1/2} \{\!\!\{ q \}\!\!\} \|_{\mathscr{F}_{\mathrm{f},h}^{\mathrm{I}}}^2 \qquad\qquad \forall q \in H^1(\mathscr{T}_{h,\mathrm{f}}),$$

$$\|\|(\boldsymbol{w}, \{q_{\mathrm{j}}\}_{\mathrm{j} \in J}, \boldsymbol{v}, p)\|\|^2 = \|\|\boldsymbol{w}\|\|_{\mathrm{D}}^2 + \sum_{\mathrm{j} \in J} \|\|q_{\mathrm{j}}\|\|_{\mathrm{P_j}}^2 + \|\|\boldsymbol{v}\|\|_{\mathrm{U}}^2 + \|\|q\|\|_{\mathrm{P_f}}^2.$$

Denoting by $\mathscr{E}_K : H^s(\Omega) \to H^s(\mathbb{R}^d)$ the Stein extension operator for a Lipschitz domain Ω defined in [49], the following interpolation result can be stated (cf. [38–40,50]):

Lemma 3. *Under Assumption 1, the following estimates hold:*

$$\forall (\boldsymbol{w}, \{q_{\mathrm{j}}\}_{\mathrm{j} \in J}, \boldsymbol{v}, q) \in [H^{m+1}(\mathscr{T}_{h,\mathrm{el}})]^{d+N_J} \times [H^{m+1}(\mathscr{T}_{h,\mathrm{f}})]^{d+1}$$
$$\exists (\boldsymbol{w}_I, \{q_{\mathrm{j}I}\}_{\mathrm{j} \in J}, \boldsymbol{v}_I, q_I) \in \boldsymbol{W}_h^{\mathrm{DG}} \times \bigtimes_{\mathrm{j} \in J} Q_{\mathrm{j},h}^{\mathrm{DG}} \times \boldsymbol{V}_h^{\mathrm{DG}} \times Q_h^{\mathrm{DG}} \quad such\ that$$

i) $\|\|(\boldsymbol{w} - \boldsymbol{w}_I, \{q_{\mathrm{j}} - q_{\mathrm{j}I}\}_{\mathrm{j} \in J}, \boldsymbol{v} - \boldsymbol{v}_I, q - q_I)\|\|^2$

$$\lesssim \sum_{K \in \mathscr{T}_{h,\mathrm{el}}} h_K^{2m} \left(\| \mathscr{E}_K \boldsymbol{w} \|_{[H^{m+1}(\hat{K})]^d}^2 + \sum_{\mathrm{j} \in J} \| \mathscr{E}_{\mathrm{j}} q_{\mathrm{j}} \|_{H^{m+1}(\hat{K})}^2 + \| \mathscr{E}_K \boldsymbol{d} \|_{[H^{m+1}(\hat{K})]^d}^2 + \| \mathscr{E}_K p \|_{H^{m+1}(\hat{K})}^2 \right),$$

ii) $\| \boldsymbol{w} \|_{\mathscr{F}^\Sigma}^2 + \sum_{\mathrm{j} \in J} \| q_{\mathrm{j}} \|_{\mathscr{F}^\Sigma}^2 + \| \boldsymbol{v} \|_{\mathscr{F}^\Sigma}^2 + \| q \|_{\mathscr{F}^\Sigma}^2$

$$\lesssim \sum_{K \in \mathscr{T}_{h,\mathrm{el}}} h_K^{2m+1} \left(\| \mathscr{E}_K \boldsymbol{w} \|_{[H^{m+1}(\hat{K})]^d}^2 + \sum_{\mathrm{j} \in J} \| \mathscr{E}_{\mathrm{j}} q_{\mathrm{j}} \|_{H^{m+1}(\hat{K})}^2 + \| \mathscr{E}_K \boldsymbol{d} \|_{[H^{m+1}(\hat{K})]^d}^2 + \| \mathscr{E}_K p \|_{H^{m+1}(\hat{K})}^2 \right),$$

where $\widehat{K} \supseteq K$, for each $K \in \mathscr{T}_h$, are shape-regular simplexes as in Assumption 1.

Combining the results above, we can prove the following optimal convergence result, whose proof is provided in Appendix C.

Theorem 4 (*A priori error estimate*). *Under the same assumptions of Theorem 1, if the solution of problem* (6) *is sufficiently regular, and the initial conditions* $\boldsymbol{d}^0, \dot{\boldsymbol{d}}^0, \boldsymbol{u}^0, p_j^0, j \in J$ *are sufficiently regular, the following estimate holds for each* $t \in (0, T]$ *and for each* $m \geq 1$:

$$
\begin{aligned}
\|(\boldsymbol{e}^{\boldsymbol{d}}, \{e^{P_j}\}_{j \in J}, &\boldsymbol{e}^{\boldsymbol{u}}, e^{P_f})\|_{\mathrm{EN},t}^2 \\
&\lesssim \sum_{K \in \mathscr{T}_{h,\mathrm{el}}} h_K^{2m} \Bigg\{ \|\mathcal{E}_K \boldsymbol{d}(t)\|_{[H^{m+1}(\widehat{K})]^d}^2 + \sum_{k \in J} \|\mathcal{E}_K p_k(t)\|_{H^{m+1}(\widehat{K})}^2 \\
&\qquad + \int_0^t \left[\|\mathcal{E}_K \partial_t \boldsymbol{d}(s)\|_{[H^{m+1}(\widehat{K})]^d}^2 + \|\mathcal{E}_K \partial_{tt}^2 \boldsymbol{d}(s)\|_{[H^{m+1}(\widehat{K})]^d}^2 \right] ds \\
&\qquad + \int_0^t \sum_{k \in J} \left(\|\mathcal{E}_K p_k(s)\|_{H^{m+1}(\widehat{K})}^2 + \|\mathcal{E}_K \partial_t p_k(s)\|_{H^{m+1}(\widehat{K})}^2 \right) ds \Bigg\} \\
&\quad + \sum_{K \in \mathscr{T}_{h,\mathrm{f}}} h_K^{2m} \int_0^t \left[\|\mathcal{E}_K \boldsymbol{u}(s)\|_{[H^{m+1}(\widehat{K})]^d}^2 + \|\mathcal{E}_K \partial_t \boldsymbol{u}(s)\|_{[H^{m+1}(\widehat{K})]^d}^2 \right. \\
&\qquad\qquad\qquad + \left. \|\mathcal{E}_K p(s)\|_{H^{m+1}(\widehat{K})}^2 \right] ds,
\end{aligned}
\tag{18}
$$

where $\boldsymbol{e}^{\boldsymbol{d}} = \boldsymbol{d} - \boldsymbol{d}_h, e^{P_j} = p_j - p_{j,h} \ \forall j \in J, \boldsymbol{e}^{\boldsymbol{u}} = \boldsymbol{u} - \boldsymbol{u}_h, e^{P_f} = p - p_h$, *and* $\widehat{K} \supseteq K$, *for each* $K \in \mathscr{T}_h$, *are shape-regular simplexes as in Assumption 1.*

5. Fully discrete problem

We introduce a uniform partition $\{t_n\}_{n=0}^N$ of the interval $(0, T)$, with constant timestep $\Delta t = t_{n+1} - t_n$, for all $n = 0, \dots N - 1$. Starting from the algebraic form of the semi-discrete problem (10), introduced in Section 3.3, we discretize the elastic momentum equation (first row) with Newmark's β-method, whereas we employ the θ-method to discretize all the compartment pressure equations and the fluid problem. For Newmark's discretization, we introduce two auxiliary vector variables $\boldsymbol{Z}^n, \boldsymbol{A}^n$ representing the expansion coefficients of the approximate elastic velocity and acceleration at time t_n. The resulting algebraic problem has the form

$$
A_1 \boldsymbol{X}^{n+1} = A_2 \boldsymbol{X}^n + \boldsymbol{F}^{n+1}, \qquad n = 1, \dots, N,
\tag{19}
$$

where

$$
\boldsymbol{X}^n = \begin{bmatrix} \boldsymbol{D}^n \\ \boldsymbol{Z}^n \\ \boldsymbol{A}^n \\ \boldsymbol{P}_{\mathrm{A}}^n \\ \vdots \\ \boldsymbol{P}_{\mathrm{E}}^n \\ \boldsymbol{U}^n \\ \boldsymbol{P}^n \end{bmatrix}, \qquad
\boldsymbol{F}^n = \begin{bmatrix} \boldsymbol{F}_{\mathrm{el}}^n \\ \boldsymbol{0} \\ \boldsymbol{0} \\ \theta \boldsymbol{F}_{\mathrm{A}}^{n+1} + (1 - \theta) \boldsymbol{F}_{\mathrm{A}}^n \\ \vdots \\ \theta \boldsymbol{F}_{\mathrm{E}}^{n+1} + (1 - \theta) \boldsymbol{F}_{\mathrm{E}}^n \\ \theta \boldsymbol{F}_{\mathrm{f}}^{n+1} + (1 - \theta) \boldsymbol{F}_{\mathrm{f}}^n \\ \boldsymbol{0} \end{bmatrix},
\tag{20}
$$

and the expression of the matrices A_1, A_2 are reported in Appendix D.

6. Verification tests – convergence

In this section, we verify the theoretical error bounds of Theorem 4. In all tests, we consider only one pressure compartment, that is $j \in J = \{E\}$. The constant coefficients of the penalty parameters defined in (8) are set as $\overline{\eta} = \overline{\zeta}_E = \overline{\gamma}_v = \overline{\gamma}_p = 10$. Regarding time discretization, all the results were obtained with $\beta = 0.25$ and $\gamma = 0.5$ for the Newmark scheme and $\theta = 0.5$ for the θ-method, both for Stokes' problem and the pressure compartment of the poro-elastic system.

The tests have been implemented in the 2D version of `lymph` (https://lymph.bitbucket.io/) [51], an open-source MATLAB library for the solution of multiphysics problems with the PolyDG method, developed at MOX, Department of Mathematics, Politecnico di Milano.
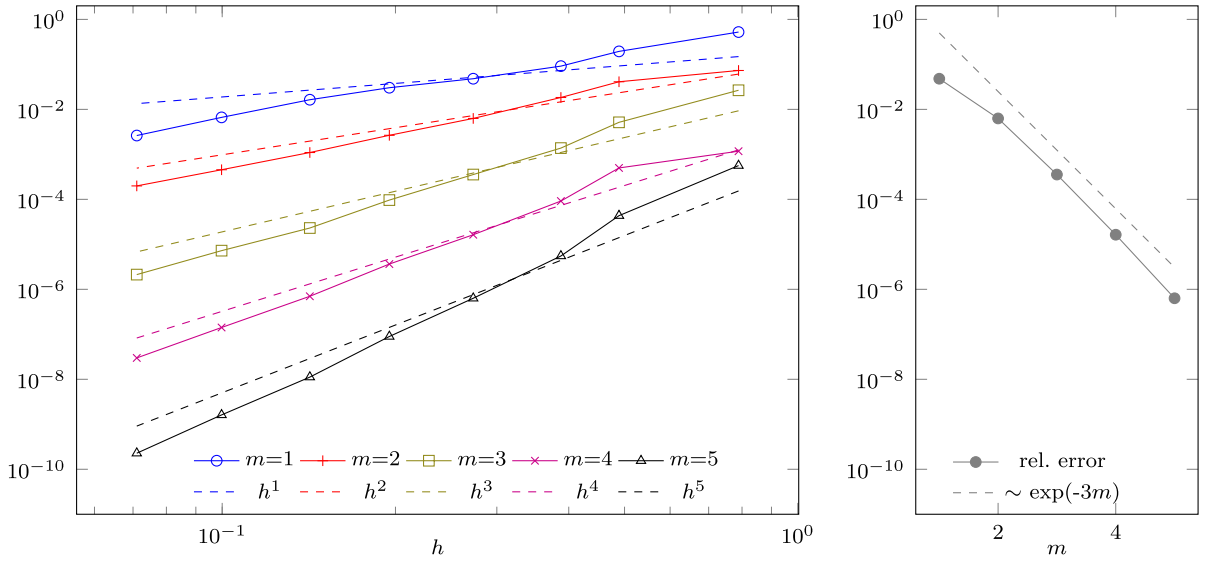
Fig. 3. Test case 1. Left: computed relative errors in the energy norm (13) versus h, for different choices of the polynomial degree $m = 1, 2, 3, 4, 5$. Right: computed relative errors in the energy norm (13) versus m, with $h = 0.273$ (corresponding to $N = 80$ polygons).

6.1. Test case 1: steady solution

In this test, we consider a manufactured steady solution of problem (1)-(2)-(3), so that we can verify the convergence of the semidiscrete formulation without spoiling the results with time discretization error. In particular, we introduce the following exact solution on the 2D domain $\Omega = \Omega_{el} \cup \Omega_f = (-1, 0) \times (0, 1) \cup (0, 1) \times (0, 1)$, with interface $\Sigma = \{0\} \times (0, 1)$ depicted in Fig. 1:

$$
\begin{aligned}
\boldsymbol{d}^{steady} &= \pi \mu \frac{K_E}{\mu_E^2}(1 - \alpha_E)(\cos(\pi x)\cos(\pi y) - \sin(\pi x)\sin(\pi y)) \begin{bmatrix} -1 \\ 1 \end{bmatrix}, \\
p_E^{steady} &= -\pi x \cos(\pi y) - 2\pi^2 \mu \frac{K_E}{\mu_E} \sin(\pi y), \\
\boldsymbol{u}^{steady} &= \pi \frac{K_E}{\mu_E}(\cos(\pi x)\cos(\pi y) - \sin(\pi x)\sin(\pi y)) \begin{bmatrix} 1 \\ -1 \end{bmatrix}, \\
p^{steady} &= -x \cos(\pi y) - 4\pi^2 \mu \frac{K_E}{\mu_E} \sin(\pi y).
\end{aligned}
\tag{21}
$$

The source terms of (1) corresponding to the exact solution above are

$$
\boldsymbol{f}_{el} = \begin{bmatrix} -2\pi^3 \mu \frac{K_E}{\mu_E}(1 - \alpha_E)(\cos(\pi x)\cos(\pi y) - \sin(\pi x)\sin(\pi y)) - \pi \alpha_E \cos(\pi y) \\ 2\pi^3 \mu \frac{K_E}{\mu_E}[(1 - \alpha_E)(\cos(\pi x)\cos(\pi y) - \sin(\pi x)\sin(\pi y)) - \alpha_E \cos(\pi y)] + \pi^2 \alpha_E x \sin(\pi y) \end{bmatrix},
$$

$$
g_E = \left(\pi^2 \frac{K_E}{\mu_E} + \beta_E^e \right) p_E,
$$

$$
\boldsymbol{f}_f = \begin{bmatrix} 2\pi^3 \mu \frac{K_E}{\mu_E}(\cos(\pi x)\cos(\pi y) - \sin(\pi x)\sin(\pi y)) - \cos(\pi y) \\ -2\pi^3 \mu \frac{K_E}{\mu_E}(\cos(\pi x)\cos(\pi y) - \sin(\pi x)\sin(\pi y) + 2\cos(\pi y)) + pi x \sin(\pi y) \end{bmatrix},
$$

and the Neumann stress on Γ_{out} is:

$$
-\overline{p}^{out}\boldsymbol{n}_f = \left(\cos(\pi y) + 6\pi^2 \mu \frac{K_E}{\mu_E} \sin(\pi y) \right) \boldsymbol{n}_f.
$$

With these data, we performed spatial convergence tests setting $\alpha_E = 0.5$ and all the physical parameters $\rho_{el}, \mu_{el}, \lambda_{el}, c_E, \mu_E, K_E, \beta_E^e$, ρ_f, μ_f equal to 1. In Fig. 3 we report the computed relative error. From the results, we can clearly observe that the error decays w.r.t. h with a rate of order m, as predicted by our theoretical estimate (18). Moreover, we can observe spectral convergence of the error w.r.t. the polynomial approximation degree m.
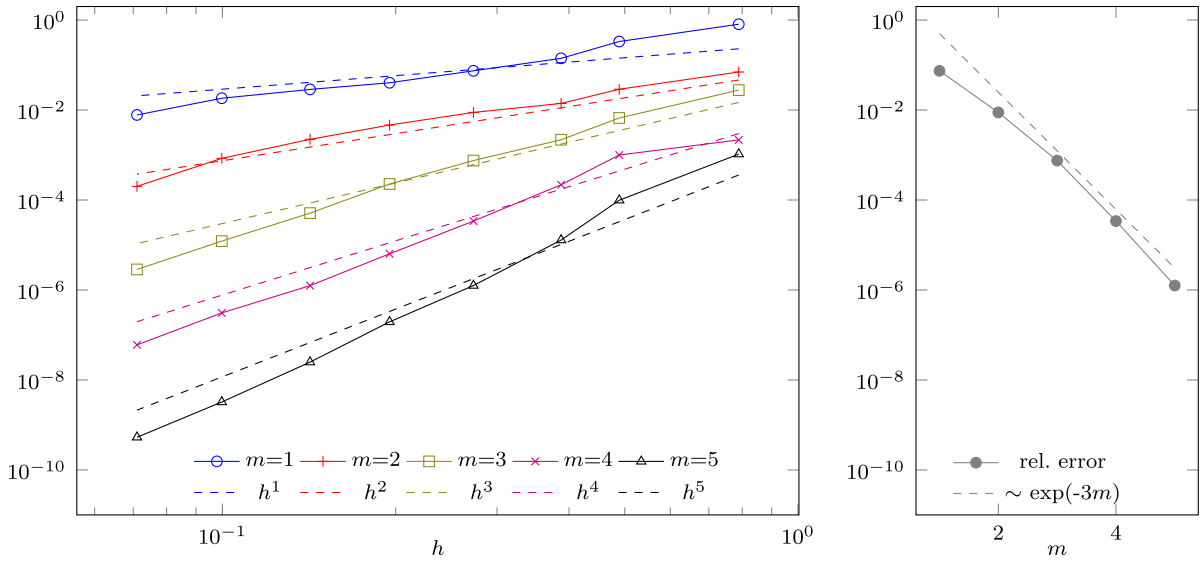
Fig. 4. Test case 2. Left: computed relative errors in the energy norm (13) versus h, with different polynomial degrees m (same for all variables). Right: computed relative errors in the energy norm (13) versus m, with $h = 0.273$ corresponding to $N = 80$ polygons.

6.2. Test case 2: unsteady solution

We consider the rectangular domain $\Omega = \Omega_{\mathrm{el}} \cup \Omega_{\mathrm{f}} = (-1,0) \times (0,1) \cup (0,1) \times (0,1)$ of Section 6.1 and we introduce the following functions of time:

$$g_{\mathrm{el}}(t) = \cos(\eta t) - \sin(\eta t), \qquad \text{where } \eta = \frac{\mu_{\mathrm{el}}}{\mu_{\mathrm{f}}(1 - \alpha_{\mathrm{E}})},$$

$$g_{\boldsymbol{u}}(t) = g_{\mathrm{el}}(t) - \frac{\dot{g}_{\mathrm{el}}(t)}{\eta}, \qquad g_p(t) = \frac{g_{\mathrm{E}}(t) + g_{\boldsymbol{u}}(t)}{2}.$$

A time-dependent exact solution of problem (1)-(2)-(3) can be manufactured by combining these functions with the steady solution introduced in Section 6.1:

$$
\begin{aligned}
\boldsymbol{d}(x,y,t) &= g_{\mathrm{el}}(t)\boldsymbol{d}^{\mathrm{steady}}(x,y), \qquad p_{\mathrm{E}}(x,y,t) = g_{\mathrm{el}}(t)p_{\mathrm{E}}^{\mathrm{steady}}(x,y), \\
\boldsymbol{u}(x,y,t) &= g_{\boldsymbol{u}}(t)\boldsymbol{u}^{\mathrm{steady}}(x,y), \qquad p(x,y,t) = g_p(t)p^{\mathrm{steady}}(x,y),
\end{aligned}
\tag{22}
$$

with suitable definitions of the source terms and boundary data. Again, we performed convergence tests setting $\alpha_{\mathrm{E}} = 0.5$ and all other physical parameters to 1. We choose a time step $\Delta t = 1 \cdot 10^{-3}$ s and a final time $T = 5\Delta t$. We report the computed relative errors in Fig. 4 (log-log scale). As predicted by Theorem 4, we observe that the error in the energy norm decays at a rate proportional to h^m, for any $m \geq 1$. Moreover, even though not covered by our theoretical analysis, we observe exponential convergence of the error for fixed h and increasing m. Finally, we observe that the value chosen for Δt is small enough to prevent error saturation for the sequence of meshes considered in this test.

7. Numerical results on a 2D slice of the brain

In this section, we demonstrate the capability of the proposed method for the solution of a realistic problem on a 2D slice of the brain and its ventricles, shown in Fig. 5. The geometry of the problem is based on structural Magnetic Resonance Images (MRI) available in the OASIS-3 database (http://oasis-brains.org) [52]. By means of the Freesurfer toolkit (http://surfer.nmr.mgh.harvard.edu/) [53], a three-dimensional brain geometry was segmented, and then sliced along the sagittal plane by VMTK (http://www.vmtk.org/) [54]. The resulting triangular 2D meshes of the cerebral tissue and of the brain ventricles surrounded by it are composed of 25847 and 3286 elements, respectively (see Fig. 5). Yet, the flexibility of the PolyDG method allows to employ meshes with elements of generic shape: by agglomeration, we can thus considerably reduce the number of mesh elements while retaining the same geometrical detail of the original triangular grid. We agglomerate the grid by means of ParMETIS (https://github.com/KarypisLab/ParMETIS) [55], obtaining the polygonal mesh shown in Fig. 5, consisting of 910 elements in $\mathcal{T}_{\mathrm{el}}$ and 101 in $\mathcal{T}_{\mathrm{f}}$. This agglomeration is performed separately for the two physical domains, to preserve geometrical accuracy at the interface Σ.

Aiming at reproducing conditions in the physiological regime, we set the data and parameters of problem (1) as follows. We split the Dirichlet boundary Γ_{w} into $\Gamma_{\mathrm{w,el}}$ representing the pia mater membrane surrounding the brain tissue and the boundary $\Gamma_{\mathrm{w,f}}$ of the corpus callosum (the whole in the center of Fig. 5). In the poroelastic problem, we consider only the compartment related to the extracellular CSF, namely $J = \{\mathrm{E}\}$, and we assume no flow ($\nabla p_{\mathrm{E}} \cdot \boldsymbol{n}_{\mathrm{el}} = 0$) through the pia mater $\Gamma_{\mathrm{w,el}}$. Notice that, for the purpose
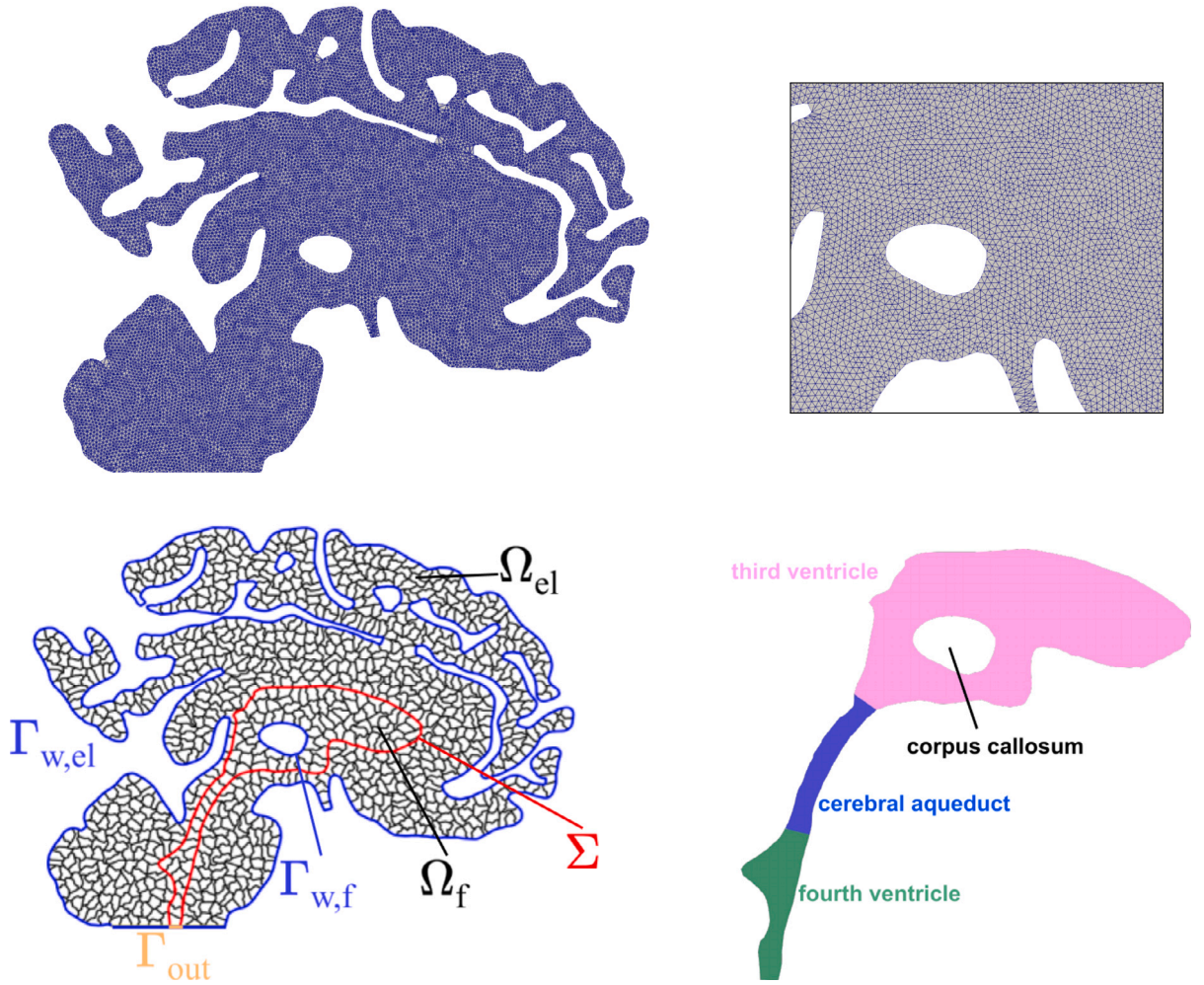
Fig. 5. Triangular mesh of the 2D slice reconstructed from MRI (top left; zoom on top right to see the triangular elements), polygonal computational mesh obtained by agglomeration (bottom left), and topographic anatomy of the fluid domain Ω_f (bottom right).

of this study, we neglect the subarachnoid space around the brain and the CSF it contains. The source of extracellular CSF is given by $g_E = 2 \cdot 10^{-3} \pi \sin(2\pi t)\mathrm{s}^{-1}$, representing the variations in the interstitial CSF due to blood pulsation [38,42], with a period of $1\,\mathrm{s}$ representing a heartbeat. No additional external forces act on the poroelastic tissue or the ventricle flow, that is $\boldsymbol{f}_{el} = \boldsymbol{f}_f = \boldsymbol{0}$. No slip conditions $\boldsymbol{u} = \boldsymbol{0}$ are enforced on $\Gamma_{w,f}$, while a no-stress condition $\overline{p}^{out} = 0$ is imposed on the obex Γ_{out} of the fourth ventricle, where the CSF would flow into the central canal of the spinal cord. Zero initial conditions are imposed on all variables and the values of the remaining physical parameters of the problem are reported in Table 1, with the slight modifications $\alpha_E = 0.49$, $\beta_E^e = 0\,\mathrm{m}^2 \cdot \mathrm{N}^{-1} \cdot \mathrm{s}^{-1}$: these values are in the physiological range of the brain function [41,42]. For the PolyDG method we employ a polynomial degree $m = 2$ for all variables and the same penalty parameters $\overline{\eta} = \overline{\zeta}_E = \overline{\gamma}_v = \overline{\gamma}_p = 10$ of Section 6, while for the time advancement based on Newmark's ($\beta = 0.25$, $\gamma = 0.5$) and Crank-Nicolson's ($\theta = 0.5$) methods we use a time step $\Delta t = 1 \cdot 10^{-2}\,\mathrm{s}$.

To ensure that our results are representative of a periodic regime of the system and independent of the initial conditions, we simulate 30 heartbeats of period $1\,\mathrm{s}$ and we assess periodicity in terms of the outlet flowrate Q and the space-averaged pressure P over the poroelastic domain. Taking both the maxima Q^i, P^i and minima Q_i, P_i over each period $i = 1, 2, \ldots, 30$, we observe that the difference between subsequent periods is less than 5% for all these quantities, for $i \geq 20$. Therefore, we deem periodicity to be reached. In the following, we discuss the results of the twentieth period.

It is worth pointing out that, despite the large ratio λ/μ_{el} between the Lamé coefficients (yielding a Poisson ratio $\nu = 0.479$) no locking phenomena were observed in the solution, in the settings described above.

Selected snapshots of the computed solutions are reported in Figs. 6 and 7. Due to the choice of a zero outlet pressure $\overline{p}^{out}$, pressures p_E, p should be interpreted as *pressure differences* (w.r.t. the fourth ventricle outflow) rather than absolute pressure values. We notice that the amplitude of the brain displacement $\boldsymbol{d}$ is always below $0.25\,\mathrm{mm}$, thus justifying the choice of a linear elasticity modeling of the tissue, at least in the current settings. Due to such small displacements, the interstitial pressure p_E at the interface and the ventricle CSF pressure p are substantially equal through the whole simulation timespan, in accordance with the interface
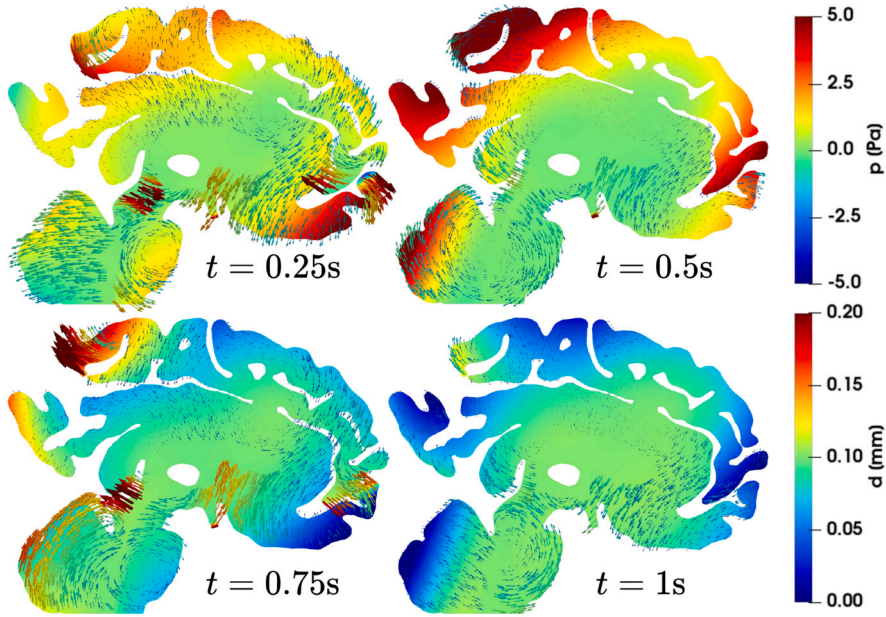
Fig. 6. Brain simulation of Section 7 (periodic regime). Discrete tissue displacement d_h and pressures $p_{E,h}, p_h$ in the whole domain $\Omega_{el} \cup \Omega_f$ at different times during a heartbeat. Same scale for $p_{E,h}, p_h$.
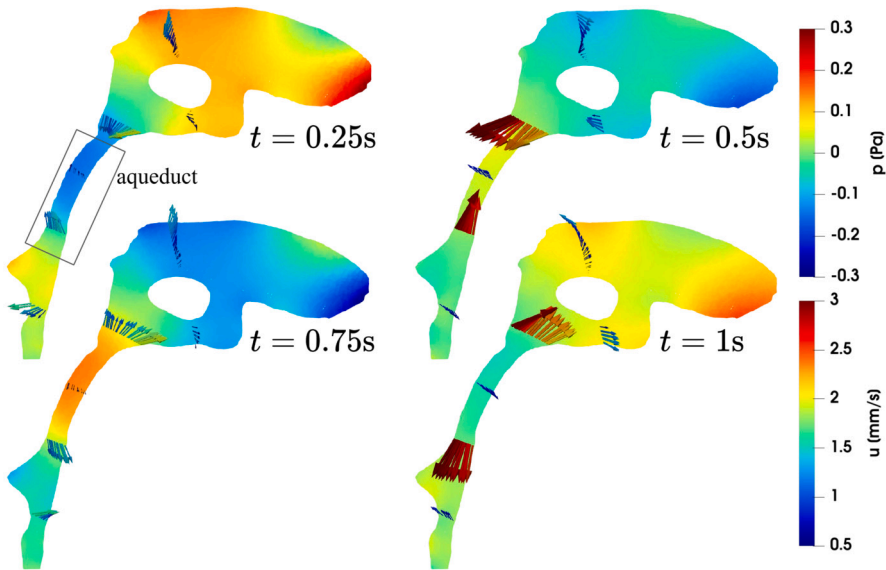

Fig. 7. Brain simulation of Section 7 (periodic regime). Velocity u_h and pressure p_h in the brain ventricles Ω_f at different times during a heartbeat. The cerebral aqueduct is indicated by the box.

conditions (3). The ventricle pressure p undergoes very small variations, which are better observable in Fig. 7. We can see that the CSF circulates in the third ventricle around the corpus callosum.

All the observations above are in general agreement with measurements and computational results in the literature. In particular, as shown in Table 2, the peak values of CSF velocity in the cerebral aqueduct and tissue displacement are in agreement with those reported in [42,56,57]. Some discrepancies with the literature can be found in the distribution of pressures p and p_E, which are underestimated. These discrepancies may be due to the fact that the computational domain of the simulation presented here is a 2D slice of the brain, and does not include the lateral ventricles: simulations in three dimensions, capturing the complete geometry of the brain, are envisaged to address this issue.

Table 2

Comparison between the values obtained in our simulation with those reported in the literature. CA: cerebral aqueduct (see Fig. 7).

quantity		computed value	literature values	references
peak $|\boldsymbol{d}|$	[mm]	0.25	0.187 ± 0.050	[42,57]
peak $|\boldsymbol{u}|$ in CA	[mm $\cdot$ s^{-1}]	17.6	$16.7 - 37.5$	[56]

8. Conclusions

We introduced a discontinuous Galerkin polytopal method for the discretization of a multiphysics fluid-mechanics model of the brain, encompassing a Multi-compartment Poro-Elastic (MPE) modeling of the tissue, perfused by blood and CSF, and Stokes' flow of the CSF in the brain cavities. Our numerical method is particularly suitable for capturing the high geometrical complexity of the brain, thanks to the possibility of supporting high-order approximations and agglomerated grids. We proved stability and optimal error bounds for the semidiscrete formulation under standard assumptions in the PolyDG framework. Specific attention was paid to the modeling and numerical treatment of the interface conditions between the MPE and fluid domain. We implemented the method in our PolyDG library `lymph` [51].

We performed verification tests, validating the optimal order of convergence of our method with respect to the mesh element size and spectral convergence with respect to the polynomial degree. Then, we showed the capability of our computational model to represent the physiological clearance function of the CSF in physiological settings, on a two-dimensional sagittal slice of the brain and of its ventricles.

Several directions for further development of the present work should be addressed. First, in terms of modeling, nonlinear hyperelastic rheology could be considered to account for the extremely soft nature of the brain tissue [58–60]. This would require more detailed fluid-structure interaction conditions on the tissue-fluid interface, which have not been fully studied in the brain ventricles, but have been widely investigated in other biological systems such as the heart and blood vessels [61–65]. Second, to thoroughly analyze the effect of the complex brain geometry on waste clearance, the model could be applied to full three-dimensional geometries of different subjects. To this aim, suitable geometry reconstruction techniques based on MRI data should be employed, such as those developed in [66–72]. Third, to better represent the effect of blood pulsation on CSF flow (here modeled by a homogeneous CSF generation term), the blood compartments of the MPE model should be coupled to models of the main brain arteries [73,74]. Finally, the coupling of the model proposed here with a suitable description of the generation, aggregation, and transport of misfolded proteins such as amyloid-β and tau, would allow the investigation of their clearance in different physiological and pathological conditions [75,76]. This would entail the development of numerical methods able to account for very different time scales, since the model presented here is defined on the scale of seconds (characteristic of blood pulsation) while prion aggregation and neurodegeneration occur over a timespan of decades.

CRediT authorship contribution statement

Ivan Fumagalli: Conceptualization, Data curation, Formal analysis, Investigation, Methodology, Software, Validation, Visualization, Writing – original draft, Writing – review & editing. **Mattia Corti:** Conceptualization, Data curation, Software, Writing – review & editing. **Nicola Parolini:** Conceptualization, Methodology, Writing – review & editing. **Paola F. Antonietti:** Conceptualization, Formal analysis, Funding acquisition, Project administration, Supervision, Writing – review & editing.

Declaration of competing interest

Data availability

Data will be made available on request.

Acknowledgement

Appendix A. Continuity and coercivity in the discrete spaces

We collect the continuity and coercivity results of [38,40] in the following Lemma, which is instrumental to the proofs of stability (Theorem 1) and convergence (Theorem 4) of our numerical method (10).

Lemma 5. *Under Assumption 1, the forms of* (7) *are continuous over the discrete spaces:*

$$|\mathcal{A}_{\mathrm{el}}(\boldsymbol{d},\boldsymbol{w})| \lesssim \|\boldsymbol{d}\|_{\mathrm{DG,D}}\|\boldsymbol{w}\|_{\mathrm{DG,D}} \qquad \forall \boldsymbol{d},\boldsymbol{w} \in \boldsymbol{W}_h^{\mathrm{DG}},$$

$$|\mathcal{A}_{\mathrm{j}}(p_{\mathrm{j}},q_{\mathrm{j}})| \lesssim \|p_{\mathrm{j}}\|_{\mathrm{DG,P_j}}\|q_{\mathrm{j}}\|_{\mathrm{DG,P_j}} \qquad \forall p_{\mathrm{j}},q_{\mathrm{j}} \in Q_{\mathrm{j},h}^{\mathrm{DG}}, \quad \mathrm{j} \in J,$$

$$\left|\sum_{\mathrm{j}\in J} C_{\mathrm{j}}(\{p_{\mathrm{k}}\}_{\mathrm{k}\in J},q_{\mathrm{j}})\right| \lesssim \sum_{\mathrm{j,k}\in J} \|p_{\mathrm{k}}\|_{\mathrm{DG,P_k}}\|q_{\mathrm{j}}\|_{\mathrm{DG,P_j}} \qquad \forall p_{\mathrm{k}},\in Q_{\mathrm{k},h}^{\mathrm{DG}}, q_{\mathrm{j}} \in Q_{\mathrm{j},h}^{\mathrm{DG}}, \quad \mathrm{j,k} \in J,$$

$$|\mathcal{B}_{\mathrm{j}}(q_{\mathrm{j}},\boldsymbol{w})| \lesssim \|q_{\mathrm{j}}\|_{\mathrm{DG,P_j}}\|\boldsymbol{w}\|_{\mathrm{DG,D}} \qquad \forall \boldsymbol{w} \in \boldsymbol{W}_h^{\mathrm{DG}}, q_{\mathrm{j}} \in Q_{\mathrm{j},h}^{\mathrm{DG}}, \quad \mathrm{j} \in J,$$

$$|\mathcal{A}_{\mathrm{f}}(\boldsymbol{u},\boldsymbol{v})| \lesssim \|\boldsymbol{u}\|_{\mathrm{DG,U}}\|\boldsymbol{v}\|_{\mathrm{DG,U}} \qquad \forall \boldsymbol{u},\boldsymbol{v} \in \boldsymbol{V}_h^{\mathrm{DG}},$$

$$|\mathcal{B}(q,\boldsymbol{v})| \lesssim \|q\|_{\mathrm{DG,P_f}}\|\boldsymbol{v}\|_{\mathrm{DG,U}} \qquad \forall \boldsymbol{v} \in \boldsymbol{V}_h^{\mathrm{DG}}, q \in Q_h^{\mathrm{DG}}.$$

Moreover, provided that the penalty constants are chosen sufficiently large, the following coercivity and inf-sup inequalities hold (for any $\mathrm{j} \in J$):

$$\mathcal{A}_{\mathrm{el}}(\boldsymbol{w},\boldsymbol{w}) \gtrsim \|\boldsymbol{w}\|_{\mathrm{DG,D}}^2 \qquad \forall \boldsymbol{w} \in \boldsymbol{W}_h^{\mathrm{DG}},$$

$$\mathcal{A}_{\mathrm{f}}(\boldsymbol{v},\boldsymbol{v}) \gtrsim \|\boldsymbol{v}\|_{\mathrm{DG,U}}^2 \qquad \forall \boldsymbol{v} \in \boldsymbol{V}_h^{\mathrm{DG}},$$

$$\sum_{\mathrm{j}\in J} C_{\mathrm{j}}(\{q_{\mathrm{k}}\}_{\mathrm{k}\in J},q_{\mathrm{j}}) \gtrsim \sum_{\mathrm{j}\in J} \|\sqrt{\beta_{\mathrm{j}}^e}q_{\mathrm{j}}\|_{DG,P_{\mathrm{j}}}^2 \quad and \quad \mathcal{A}_{\mathrm{j}}(q_{\mathrm{j}},q_{\mathrm{j}}) \gtrsim \|q_{\mathrm{j}}\|_{\mathrm{DG,P_j}}^2 \quad \forall q_{\mathrm{j}} \in Q_{\mathrm{j},h}^{\mathrm{DG}}, \mathrm{j} \in J,$$

$$\sup_{\boldsymbol{v}\in \boldsymbol{V}_h^{\mathrm{DG}}\backslash\{0\}} \frac{\mathcal{B}_{\mathrm{f}}(q,\boldsymbol{v})}{\|\boldsymbol{v}\|_{\mathrm{DG,U}}} + \sqrt{S(q,q)} \geq \beta_{\mathrm{f},h}\|q\|_{\Omega_{\mathrm{f}}} \qquad \forall q \in Q_h^{\mathrm{DG}},$$

where $\beta_{\mathrm{f},h}$ *is the discrete inf-sup constant [40].*

Appendix B. Proof of Theorem 2

Let $q \in H^2(\mathcal{T}_{h,\mathrm{el}}), \boldsymbol{w} \in H^2(\mathcal{T}_{h,\mathrm{el}}), \boldsymbol{v} \in H^2(\mathcal{T}_{h,\mathrm{f}})$, and $q \in Q_{\mathrm{E},h}^{\mathrm{DG}}, \boldsymbol{w}_h \in \boldsymbol{W}_h^{\mathrm{DG}}, \boldsymbol{v}_h \in \boldsymbol{V}_h^{\mathrm{DG}}$. For any $F \in \mathcal{F}_h^{\Sigma}$, we denote by K_{el}^F and K_{f}^F the elements of $\mathcal{T}_{h,\mathrm{el}}$ and $\mathcal{T}_{h,\mathrm{f}}$, respectively, sharing F in their boundary. Then,

$$|\mathcal{J}(q,\boldsymbol{w}_h,\boldsymbol{v}_h)| \leq \sum_{F\in\mathcal{F}_h^{\Sigma}} \left(\left|\int_F q\,\boldsymbol{w}_h \cdot \boldsymbol{n}_{\mathrm{el}}\right| + \left|\int_F q\,\boldsymbol{v}_h \cdot \boldsymbol{n}_{\mathrm{f}}\right|\right)$$

$$\lesssim \sum_{F\in\mathcal{F}_h^{\Sigma}} \left(\|\eta^{1/2}q\|_F \|\eta^{-1/2}\boldsymbol{w}_h\|_F + \|\gamma_p^{-1/2}q\|_F \|\gamma_p^{1/2}\boldsymbol{v}_h\|_F\right)$$

$$\overset{\boxed{\mathrm{TR}}}{\lesssim} \sum_{F\in\mathcal{F}_h^{\Sigma}} \left(\|\eta^{1/2}q\|_F h_{K_{\mathrm{el}}^F}^{1/2} h_{K_{\mathrm{el}}^F}^{-1/2}\|\boldsymbol{w}_h\|_{K_{\mathrm{el}}^F} + \|\gamma_p^{-1/2}q\|_F h_{K_{\mathrm{f}}^F}^{1/2} h_{K_{\mathrm{f}}^F}^{-1/2}\|\boldsymbol{v}_h\|_{K_{\mathrm{f}}^F}\right)$$

$$\leq \|\eta^{1/2}q\|_{\mathcal{F}_h^{\Sigma}}\|\boldsymbol{w}_h\|_{\mathrm{DG,D}} + \|\gamma_p^{-1/2}q\|_{\mathcal{F}_h^{\Sigma}}\|\boldsymbol{v}_h\|_{\mathrm{DG,U}},$$

where, in line $\boxed{\text{TR}}$, we have used the inverse trace inequality (17) and the fact that $\eta|_K \sim h_K^{-1} \; \forall K \in \mathscr{T}_{h,\text{el}}$ and $\gamma_p|_K \sim h_K \; \forall K \in \mathscr{T}_{h,\text{f}}$. An analogous argument (using $\gamma_v^{1/2}$ in place of $\gamma_p^{-1/2}$) allows to control $|J(q_h, \boldsymbol{w}, \boldsymbol{v})|$, thus concluding the proof.

Appendix C. Proof of Theorem 4

In this section, we prove the optimal convergence estimate stated in Theorem 4. This result is based on the inverse trace inequality (17), on Theorem 2 and on the following continuity results (proved in [31,39,40]), which extend Theorem 5 to consider also non-discrete functions:

Lemma 6. *Under the same assumptions of Theorem 5, the following inequalities hold:*

$$|\mathcal{A}_{\text{el}}(\boldsymbol{d}, \boldsymbol{w}_h)| \lesssim |\!|\!|\boldsymbol{d}|\!|\!|_{\text{D}} \|\boldsymbol{w}_h\|_{\text{DG,D}} \qquad \forall \boldsymbol{d} \in [H^2(\mathscr{T}_{h,\text{el}})]^d, \boldsymbol{w}_h \in \boldsymbol{W}_h^{\text{DG}},$$

$$|\mathcal{A}_{\text{j}}(p_{\text{j}}, q_{\text{j},h})| \lesssim |\!|\!|p_{\text{j}}|\!|\!|_{\text{P}_{\text{j}}} \|q_{\text{j},h}\|_{\text{DG,P}_{\text{j}}} \qquad \forall p_{\text{j}} \in H^2(\mathscr{T}_{h,\text{el}}), q_{\text{j},h} \in Q_{\text{j},h}^{\text{DG}}, \quad \forall \text{j} \in J,$$

$$|\mathcal{B}_{\text{j}}(q_{\text{j},h}, \boldsymbol{w})| \lesssim \|q_{\text{j},h}\|_{\text{DG,P}_{\text{j}}} |\!|\!|\boldsymbol{w}|\!|\!|_{\text{D}} \qquad \forall \boldsymbol{w} \in [H^2(\mathscr{T}_{h,\text{el}})]^d, q_{\text{j},h} \in Q_{\text{j},h}^{\text{DG}}, \quad \forall \text{j} \in J,$$

$$|\mathcal{B}_{\text{j}}(q_{\text{j}}, \boldsymbol{w}_h)| \lesssim |\!|\!|q_{\text{j}}|\!|\!|_{\text{P}_{\text{j}}} \|\boldsymbol{w}_h\|_{\text{DG,D}} \qquad \forall \boldsymbol{w}_h \in \boldsymbol{W}_h^{\text{DG}}, q_{\text{j}} \in H^2(\mathscr{T}_{h,\text{el}}), \quad \forall \text{j} \in J,$$

$$|\mathcal{A}_{\text{f}}(\boldsymbol{u}, \boldsymbol{v}_h)| \lesssim |\!|\!|\boldsymbol{u}|\!|\!|_{\text{U}} \|\boldsymbol{v}_h\|_{\text{DG,U}} \qquad \forall \boldsymbol{u} \in [H^2(\mathscr{T}_{h,\text{f}})]^d, \boldsymbol{v}_h \in \boldsymbol{V}_h^{\text{DG}},$$

$$|\mathcal{B}_{\text{f}}(q_h, \boldsymbol{v})| \lesssim \|q_h\|_{\text{DG,P}_{\text{f}}} |\!|\!|\boldsymbol{v}|\!|\!|_{\text{U}} \qquad \forall \boldsymbol{v} \in [H^2(\mathscr{T}_{h,\text{f}})]^d, q_h \in Q_h^{\text{DG}},$$

$$|\mathcal{B}_{\text{f}}(q, \boldsymbol{v}_h)| \lesssim |\!|\!|q|\!|\!|_{\text{P}_{\text{f}}} \|\boldsymbol{v}_h\|_{\text{DG,U}} \qquad \forall \boldsymbol{v}_h \in \boldsymbol{V}_h^{\text{DG}}, q \in H^1(\mathscr{T}_{h,\text{f}}).$$

We are now ready to prove our optimal convergence result.

Proof. (Theorem 4) Using the interpolators defined in Theorem 3, we split the error $e^{\boldsymbol{d}} = e_I^{\boldsymbol{d}} - e_h^{\boldsymbol{d}}$ into an interpolation error $e_I^{\boldsymbol{d}} = \boldsymbol{d} - \boldsymbol{d}_I \in [H^{m+1}(\mathscr{T}_{h,\text{el}})]^d$ and an approximation error $e_h^{\boldsymbol{d}} = \boldsymbol{d}_h - \boldsymbol{d}_I \in \boldsymbol{W}_h^{\text{DG}}$. An analogous notation is introduced for the errors $e^{P_{\text{j}}} \forall \text{j} \in J, e^{\boldsymbol{u}}, e^{P_{\text{f}}}$. We fix a time $t \in (0, T]$ and we proceed similarly to [38], namely we subtract equation (10) from (6), tested against $(\partial_t e_h^{\boldsymbol{d}}, \{e_h^{P_{\text{j}}}\}_{\text{j} \in J}, e_h^{\boldsymbol{u}}, e_h^{P_{\text{f}}})$, thus obtaining

$$(\rho_{\text{el}} \partial_{tt}^2 e^{\boldsymbol{d}}, \partial_t e_h^{\boldsymbol{d}})_{\Omega_{\text{el}}} + \mathcal{A}_{\text{el}}(e^{\boldsymbol{d}}, \partial_t e_h^{\boldsymbol{d}}) + \sum_{\text{k} \in J} \mathcal{B}_{\text{k}}(e^{P_{\text{k}}}, \partial_t e_h^{\boldsymbol{d}})$$

$$+ \sum_{\text{j} \in J} \left[(c_{\text{j}} \partial_t e^{P_{\text{j}}}, e_h^{P_{\text{j}}})_{\Omega_{\text{el}}} + \mathcal{A}_{\text{j}}(e^{P_{\text{j}}}, e_h^{P_{\text{j}}}) + C_{\text{j}}(\{e^{P_{\text{k}}}\}_{\text{k} \in J}, e_h^{P_{\text{j}}}) - \mathcal{B}_{\text{j}}(e_h^{P_{\text{j}}}, \partial_t e^{\boldsymbol{d}}) \right]$$

$$+ (\rho_{\text{f}} \partial_t e^{\boldsymbol{u}}, \boldsymbol{u}_h)_{\Omega_{\text{f}}} + \mathcal{A}_{\text{f}}(e^{\boldsymbol{u}}, e_h^{\boldsymbol{u}}) + \mathcal{B}_{\text{f}}(e^{P_{\text{f}}}, e_h^{\boldsymbol{u}}) - \mathcal{B}_{\text{f}}(e_h^{P_{\text{f}}}, e^{\boldsymbol{u}}) + S(e^{P_{\text{f}}}, e_h^{P_{\text{f}}})$$

$$+ \mathcal{J}(e^{P_{\text{E}}}, \partial_t e_h^{\boldsymbol{d}}, e_h^{\boldsymbol{u}}) - \mathcal{J}(e_h^{P_{\text{E}}}, \partial_t e^{\boldsymbol{d}}, e^{\boldsymbol{u}}) = 0.$$

According to the splitting introduced above, we separate the terms depending only on the discrete approximation errors from those involving the interpolation errors. Then, integrating in time from 0 to t and proceeding as in the proof of Theorem 1, the coercivity inequalities of Theorem 5 yield

$$\|\sqrt{\rho_{\text{el}}} \partial_t e_h^{\boldsymbol{d}}\|_{\Omega_{\text{el}}}^2 + \|e_h^{\boldsymbol{d}}\|_{\text{DG,D}}^2 + \sum_{\text{k} \in J} \left[\|\sqrt{c_{\text{k}}} e_h^{P_{\text{k}}}\|_{\Omega_{\text{el}}}^2 + \int_0^t \left(\|e_h^{P_{\text{k}}}\|_{\text{DG,P}_{\text{k}}}^2 + \|\sqrt{\beta_{\text{k}}^e} e_h^{P_{\text{k}}}\|_{\Omega_{\text{el}}}^2 \right) ds \right]$$

$$+ \|\sqrt{\rho_{\text{f}}} e_h^{\boldsymbol{u}}\|_{\Omega_{\text{f}}}^2 + \int_0^t \alpha \left(\|e_h^{\boldsymbol{u}}\|_{\text{DG,U}}^2 + \|e_h^{P_{\text{f}}}\|_{\text{DG,P}_{\text{f}}}^2 \right) ds$$

$$+ \int_0^t \left[\cancel{\mathcal{J}(e_h^{P_{\text{E}}}, \partial_t e_h^{\boldsymbol{d}}, e_h^{\boldsymbol{u}})} - \cancel{\mathcal{J}(e_h^{P_{\text{E}}}, \partial_t e_h^{\boldsymbol{d}}, e_h^{\boldsymbol{u}})} \right] ds$$

$$\lesssim \int_0^t (\rho_{\text{el}} \partial_{tt}^2 e_I^{\boldsymbol{d}}, \partial_t e_h^{\boldsymbol{d}})_{\Omega_{\text{el}}} ds + \mathcal{A}_{\text{el}}(e_I^{\boldsymbol{d}}, e_h^{\boldsymbol{d}}) - \int_0^t \mathcal{A}_{\text{el}}(\partial_t e_I^{\boldsymbol{d}}, e_h^{\boldsymbol{d}}) ds \qquad (\text{C.1})$$

$$+ \sum_{\text{k} \in J} \int_0^t \left[(c_{\text{k}} \partial_t e_I^{P_{\text{k}}}, e_h^{P_{\text{k}}})_{\Omega_{\text{el}}} + \mathcal{A}_{\text{k}}(e_I^{P_{\text{k}}}, e_h^{P_{\text{k}}}) + C_{\text{k}}(\{e_I^{P_{\text{j}}}\}_{\text{j} \in J}, e_h^{P_{\text{k}}}) \right] ds$$

$$+ \sum_{k \in J} \mathcal{B}_k(e_I^{P_k}, e_h^d) - \sum_{k \in J} \int_0^t \left[\mathcal{B}_k(e_I^{P_k}, \partial_t e_h^d) + \mathcal{B}_k(e_h^{P_k}, \partial_t e_I^d) \right] ds$$

$$+ \int_0^t \left[(\rho_f \partial_t e_I^u, e_h^u)_{\Omega_f} + \mathcal{A}_f(e_I^u, e_h^u) + \mathcal{B}_f(e_I^{P_f}, e_h^u) - \mathcal{B}_f(e_h^{P_f}, e_I^u) + \mathcal{S}(e_I^{P_f}, e_h^{P_f}) \right] ds$$

$$+ \int_0^t \left[J(e_I^{P_E}, \partial_t e_h^d, e_h^u) - J(e_h^{P_E}, \partial_t e_I^d, e_I^u) \right] ds,$$

where no contribution arises from the initial conditions, due to the hypotheses. Using Theorems 2 and 6 and the inequality

$$\sum_{k \in J} |C_k(\{e_I^{P_j}\}_{j \in J}, e_h^{P_k})| \lesssim \sum_{j,k \in J} \|c_j^{-1/2} e_I^{P_j}\|_{\Omega_{el}} \|\sqrt{c_k} e_h^{P_k}\|_{\Omega_{el}} \lesssim \sum_{j,k \in J} \|e_I^{P_j}\|_{P_j} \|\sqrt{c_k} e_h^{P_k}\|_{\Omega_{el}}$$

on the right-hand side of (C.1) yields

$$\|(e_h^d, \{e_h^{P_j}\}_{j \in J}, e_h^u, e_h^{P_f})\|_{EN,t}^2$$

$$\lesssim \|\!|e_I^d(t)|\!|_D \|e_h^d(t)\|_{DG,D} + \int_0^t \left[\|\sqrt{\rho_{el}} \partial_{tt}^2 e_I^d(s)\|_{\Omega_{el}} \|\sqrt{\rho_{el}} \partial_t e_h^d(s)\|_{\Omega_{el}} \right.$$

$$\left. + \|\!|\partial_t e_I^d(s)|\!|_D \|e_h^d(s)\|_{DG,D} \right] ds$$

$$+ \sum_{k \in J} \left[\|\!|e_I^{P_k}(t)|\!|_{P_k} \|e_h^d(t)\|_{DG,D} + \int_0^t \|\sqrt{c_k} \partial_t e_I^{P_k}(s)\|_{\Omega_{el}} \|\sqrt{c_k} e_h^{P_k}(s)\|_{\Omega_{el}} ds \right]$$

$$+ \sum_{k \in J} \int_0^t \left[\|\!|e_I^{P_k}(s)|\!|_{P_k} \|\!|e_h^{P_k}(s)|\!|_{DG,P_k} + \|\!|e_I^{P_k}(s)|\!|_{P_k} \|\partial_t e_h^d(s)\|_{DG,D} \right] ds$$

$$+ \sum_{k \in J} \int_0^t \left[\|e_h^{P_k}(s)\|_{DG,P_k} \|\!|\partial_t e_I^d(s)|\!|_D + \sum_{j \in J} \|\!|e_I^{P_j}(s)|\!|_{P_j} \|\sqrt{c_k} e_h^{P_k}(s)\|_{\Omega_{el}} \right] ds \qquad \text{(C.2)}$$

$$+ \int_0^t [\|\sqrt{\rho_f} \partial_t e_I^u(s)\|_{\Omega_f} \|e_h^u(s)\|_{\Omega_f} + \|\!|e_I^u(s)|\!|_U \|e_h^u(s)\|_{DG,U}$$

$$+ \|\!|e_I^{P_f}(s)|\!|_{P_f} \|e_h^u(s)\|_{DG,U}] ds$$

$$+ \int_0^t \left[\|e_h^{P_f}(s)\|_{DG,P_f} \|\!|e_I^u(s)|\!|_U + \sqrt{\mathcal{S}(e_I^{P_f}(s), e_I^{P_f}(s))} \sqrt{\mathcal{S}(e_h^{P_f}(s), e_h^{P_f}(s))} \right] ds$$

$$+ \int_0^t \left[\|\eta^{1/2} e_I^{P_E}\|_{\mathscr{F}_h^\Sigma} \|\partial_t e_h^d\|_{DG,D} + \|\gamma_p^{-1/2} e_I^{P_E}\|_{\mathscr{F}_h^\Sigma} \|e_h^u\|_{DG,U} \right] ds$$

$$+ \int_0^t \left[\|e_h^{P_E}\|_{DG,P_E} \left(\|\eta^{1/2} \partial_t e_I^d\|_{\mathscr{F}_h^\Sigma} + \|\gamma_v^{1/2} e_I^u\|_{\mathscr{F}_h^\Sigma} \right) \right] ds.$$

Regarding the interface terms, we can observe that the choice of η, γ_v, γ_p made in (8) implies that $\eta, \gamma_v, \gamma_p^{-1}$ scale as h_K in each element $K \in \mathscr{T}_h$. Thus, thanks to Theorem 3, we obtain

$$\|\eta^{1/2} e_I^{P_E}\|_{\mathscr{F}_h^\Sigma} \lesssim \sum_{K \in \mathscr{T}_{h,el}} \|\eta\|_{L^\infty(K)}^{1/2} \|h_K^{m+1/2}\|\mathcal{E}_K p_E\|_{H^{m+1}(\hat{K})} \lesssim \sum_{K \in \mathscr{T}_{h,el}} h_K^m \|\mathcal{E}_K p_E\|_{H^{m+1}(\hat{K})},$$

and similar optimal estimates for the other interpolation errors at the interface appearing in the last two lines of (C.2).

By Cauchy-Schwarz's and Young's inequalities, all the terms involving the discrete errors $e_h^d, e_h^{P_j}, e_h^u, e_h^{P_f}$ on the right-hand side of (C.2) can be moved to the left-hand side, whereas the interpolation errors $e_I^d, e_I^{P_j}, e_I^u, e_I^{P_f}$ can be controlled by the estimates of Theorem 3, yielding

$$\|(e_h^d, \{e_h^{P_j}\}_{j \in J}, e_h^u, e_h^{P_f})\|_{EN,t}^2$$

$$\lesssim \sum_{K \in \mathcal{T}_{h,\mathrm{el}}} \frac{h_K^{2m}}{m} \left\{ \|\mathcal{E}_K \boldsymbol{d}(t)\|^2_{[H^{m+1}(\hat{K})]^d} + \sum_{\mathrm{k} \in J} \|\mathcal{E}_K p_\mathrm{k}(t)\|^2_{H^{m+1}(\hat{K})} \right.$$

$$+ \int_0^t \left[\|\mathcal{E}_K \partial_t \boldsymbol{d}(s)\|^2_{[H^{m+1}(\hat{K})]^d} + \|\mathcal{E}_K \partial_{tt}^2 \boldsymbol{d}(s)\|^2_{[H^{m+1}(\hat{K})]^d} \right. \tag{C.3}$$

$$\left. \left. + \sum_{\mathrm{k} \in J} \left(\|\mathcal{E}_K p_\mathrm{k}(s)\|^2_{H^{m+1}(\hat{K})} + \|\mathcal{E}_K \partial_t p_\mathrm{k}(s)\|^2_{H^{m+1}(\hat{K})} \right) \right] ds \right\}$$

$$+ \sum_{K \in \mathcal{T}_{h,\mathrm{f}}} \frac{h_K^{2m}}{m} \int_0^t \left[\|\mathcal{E}_K \boldsymbol{u}(s)\|^2_{[H^{m+1}(\hat{K})]^d} + \|\mathcal{E}_K \partial_t \boldsymbol{u}(s)\|^2_{[H^{m+1}(\hat{K})]^d} \right.$$

$$\left. + \|\mathcal{E}_K p(s)\|^2_{H^{m+1}(\hat{K})} \right] ds.$$

Observing that an estimate for $\|(e_I^{\boldsymbol{d}}, \{e_I^{P_\mathrm{j}}\}_{\mathrm{j} \in J}, e_I^{\boldsymbol{u}}, e_I^{P_\mathrm{f}})\|_{\mathrm{EN},t}$ that is completely analogous to (C.3) can be proven by resorting to Theorem 3, the triangle inequality

$$\|(e^{\boldsymbol{d}}, \{e^{P_\mathrm{j}}\}_{\mathrm{j} \in J}, e^{\boldsymbol{u}}, e^{P_\mathrm{f}})\|^2_{\mathrm{EN},t} \le \|(e_h^{\boldsymbol{d}}, \{e_h^{P_\mathrm{j}}\}_{\mathrm{j} \in J}, e_h^{\boldsymbol{u}}, e_h^{P_\mathrm{f}})\|^2_{\mathrm{EN},t} + \|(e_I^{\boldsymbol{d}}, \{e_I^{P_\mathrm{j}}\}_{\mathrm{j} \in J}, e_I^{\boldsymbol{u}}, e_I^{P_\mathrm{f}})\|^2_{\mathrm{EN},t}$$

concludes the proof. □

Appendix D. Algebraic form of the fully discrete problem

The matrices A_1, A_2 of (19) have the following form:

$$A_1 = \begin{bmatrix}
A_\mathrm{el} & 0 & M_\mathrm{el} & B_\mathrm{A}^T & \cdots & B_\mathrm{E}^T + J_\mathrm{el}^T & 0 & 0 \\
0 & I & -\gamma \Delta t I & 0 & \cdots & 0 & 0 & 0 \\
-\frac{1}{\beta \Delta t^2} I & 0 & I & 0 & \cdots & 0 & 0 & 0 \\
-\frac{\theta \gamma}{\beta \Delta t} B_\mathrm{A} & 0 & 0 & \theta K_\mathrm{AA} & \cdots & \theta C_\mathrm{AE} & 0 & 0 \\
\vdots & \vdots & \vdots & \vdots & \vdots & \vdots & \vdots & \vdots \\
-\frac{\theta \gamma}{\beta \Delta t}(B_\mathrm{E} + J_\mathrm{el}) & & & \theta C_\mathrm{EA} & \cdots & \theta K_\mathrm{EE} & -\theta J_\mathrm{f} & 0 \\
0 & 0 & 0 & 0 & \cdots & \theta J_\mathrm{f}^T & \frac{1}{\Delta t} M_\mathrm{f} + \theta A_\mathrm{f} & \theta B_\mathrm{f}^T \\
0 & 0 & 0 & 0 & \cdots & 0 & -\theta B_\mathrm{f} & \theta S
\end{bmatrix},$$

$$A_2 = \begin{bmatrix}
0 & 0 & 0 & 0 & \cdots & 0 & 0 & 0 \\
0 & I & (1-\gamma)\Delta t I & 0 & \cdots & 0 & 0 & 0 \\
-\frac{1}{\beta \Delta t^2} I & -\frac{1}{\beta \Delta t} I & \frac{2\beta-1}{2\beta} I & 0 & \cdots & 0 & 0 & 0 \\
-\frac{\theta \gamma}{\beta \Delta t} B_\mathrm{A} & \left(1 - \frac{\theta \gamma}{\beta}\right) B_\mathrm{A} & \theta \Delta t \left(1 - \frac{\gamma}{2\beta}\right) B_\mathrm{A} & \frac{1}{\Delta t} M_\mathrm{A} - \overline{\theta} K_\mathrm{AA} & \cdots & \overline{\theta} C_\mathrm{AE} & 0 & 0 \\
\vdots & \vdots & \vdots & \vdots & \vdots & \vdots & & \\
-\frac{\theta \gamma}{\beta \Delta t}(B_\mathrm{E} + J_\mathrm{el}) & \left(1 - \frac{\theta \gamma}{\beta}\right) B_\mathrm{E} & \theta \Delta t \left(1 - \frac{\gamma}{2\beta}\right) B_\mathrm{E} & \overline{\theta} C_\mathrm{EA} & \cdots & \frac{1}{\Delta t} M_\mathrm{E} + \overline{\theta} K_\mathrm{EE} & -\overline{\theta} J_\mathrm{f} & 0 \\
0 & 0 & 0 & 0 & \cdots & \overline{\theta} J_\mathrm{f}^T & \frac{1}{\Delta t} M_\mathrm{f} + \overline{\theta} A_\mathrm{f} & \overline{\theta} B_\mathrm{f}^T \\
0 & 0 & 0 & 0 & \cdots & 0 & -\overline{\theta} B_\mathrm{f} & \overline{\theta} S
\end{bmatrix}$$

where $\overline{\theta} = 1 - \theta, \qquad K_\mathrm{jj} = A_\mathrm{j} + C_\mathrm{jj} \quad \forall \mathrm{j} \in J.$

References

[1] L.M. Hablitz, M. Nedergaard, The glymphatic system, Curr. Biol. 31 (20) (2021) R1371–R1375.

[2] T. Bohr, P.G. Hjorth, S.C. Holst, S. Hrabětová, V. Kiviniemi, T. Lilius, I. Lundgaard, K.-A. Mardal, E.A. Martens, Y. Mori, et al., The glymphatic system: current understanding and modeling, iScience 25 (9) (2022).

[3] A. Bacyinski, M. Xu, W. Wang, J. Hu, The paravascular pathway for brain waste clearance: current understanding, significance and controversy, Front. Neuroanatom. 11 (2017) 101.

[4] T.M. Kylkilahti, E. Berends, M. Ramos, N.C. Shanbhag, J. Töger, K. Markenroth Bloch, I. Lundgaard, Achieving brain clearance and preventing neurodegenerative diseases—a glymphatic perspective, J. Cereb. Blood Flow Metab. 41 (9) (2021) 2137–2149.

[5] K. Gouveia-Freitas, A.J. Bastos-Leite, Perivascular spaces and brain waste clearance systems: relevance for neurodegenerative and cerebrovascular pathology, Neuroradiology 63 (10) (2021) 1581–1597.

[6] G.S. Brennan, T.B. Thompson, H. Oliveri, M.E. Rognes, A. Goriely, The role of clearance in neurodegenerative diseases, SIAM J. Appl. Math. (2023) S172–S198.

[7] T. Brinker, E. Stopa, J. Morrison, P. Klinge, A new look at cerebrospinal fluid circulation, Fluids Barriers CNS 11 (1) (2014) 1–16.

[8] O. Zienkiewicz, T. Shiomi, Dynamic behaviour of saturated porous media; the generalized Biot formulation and its numerical solution, Int. J. Numer. Anal. Methods Geomech. 8 (1) (1984) 71–96.

[9] A.A. Linninger, K. Tangen, C.-Y. Hsu, D. Frim, Cerebrospinal fluid mechanics and its coupling to cerebrovascular dynamics, Annu. Rev. Fluid Mech. 48 (2016) 219–257.

[10] S. Badia, A. Quaini, A. Quarteroni, Coupling Biot and Navier–Stokes equations for modelling fluid–poroelastic media interaction, J. Comput. Phys. 228 (21) (2009) 7986–8014.

[11] I. Ambartsumyan, E. Khattatov, I. Yotov, P. Zunino, A Lagrange multiplier method for a Stokes–Biot fluid–poroelastic structure interaction model, Numer. Math. 140 (2) (2018) 513–553.

[12] C. Ager, B. Schott, M. Winter, W.A. Wall, A Nitsche-based cut finite element method for the coupling of incompressible fluid flow with poroelasticity, Comput. Methods Appl. Mech. Eng. 351 (2019) 253–280.

[13] W.M. Boon, M. Hornkjøl, M. Kuchta, K.-A. Mardal, R. Ruiz-Baier, Parameter-robust methods for the Biot–Stokes interfacial coupling without Lagrange multipliers, J. Comput. Phys. 467 (2022) 111464.

[14] L. Bociu, S. Canic, B. Muha, J.T. Webster, Multilayered poroelasticity interacting with Stokes flow, SIAM J. Math. Anal. 53 (6) (2021) 6243–6279.

[15] M. Bukač, I. Yotov, P. Zunino, An operator splitting approach for the interaction between a fluid and a multilayered poroelastic structure, Numer. Methods Partial Differ. Equ. 31 (4) (2015) 1054–1100.

[16] A. Dereims, S. Drapier, J.-M. Bergheau, P. De Luca, 3D robust iterative coupling of Stokes, Darcy and solid mechanics for low permeability media undergoing finite strains, Finite Elem. Anal. Des. 94 (2015) 1–15.

[17] S. Di Gregorio, M. Fedele, G. Pontone, A.F. Corno, P. Zunino, C. Vergara, A. Quarteroni, A computational model applied to myocardial perfusion in the human heart: from large coronaries to microvasculature, J. Comput. Phys. 424 (2021) 109836.

[18] N.A. Barnafi Wittwer, S.D. Gregorio, L. Dede', P. Zunino, C. Vergara, A. Quarteroni, A multiscale poromechanics model integrating myocardial perfusion and the epicardial coronary vessels, SIAM J. Appl. Math. 82 (4) (2022) 1167–1193.

[19] B. Tully, Y. Ventikos, Cerebral water transport using multiple-network poroelastic theory: application to normal pressure hydrocephalus, J. Fluid Mech. 667 (2011) 188–215.

[20] D. Chou, J.C. Vardakis, L. Guo, B.J. Tully, Y. Ventikos, A fully dynamic multi-compartmental poroelastic system: application to aqueductal stenosis, J. Biomech. 49 (11) (2016) 2306–2312.

[21] A. Quarteroni, Numerical Models for Differential Problems, vol. 2, Springer, 2009.

[22] E. Godlewski, P.-A. Raviart, Numerical Approximation of Hyperbolic Systems of Conservation Laws, vol. 118, Springer Science & Business Media, 2013.

[23] F. Bassi, L. Botti, A. Colombo, D.A. Di Pietro, P. Tesini, On the flexibility of agglomeration based physical space discontinuous Galerkin discretizations, J. Comput. Phys. 231 (1) (2012) 45–65.

[24] A. Cangiani, E.H. Georgoulis, P. Houston, Hp-version discontinuous Galerkin methods on polygonal and polyhedral meshes, Math. Models Methods Appl. Sci. 24 (10) (2014) 2009–2041.

[25] P.F. Antonietti, A. Cangiani, J. Collis, Z. Dong, E.H. Georgoulis, S. Giani, P. Houston, Review of discontinuous Galerkin finite element methods for partial differential equations on complicated domains, in: Building Bridges: Connections and Challenges in Modern Approaches to Numerical Partial Differential Equations, 2016, pp. 281–310.

[26] A. Cangiani, Z. Dong, E.H. Georgoulis, P. Houston, Hp-Version Discontinuous Galerkin Methods on Polygonal and Polyhedral Meshes, Springer, 2017.

[27] W. Pazner, P.-O. Persson, On the convergence of iterative solvers for polygonal discontinuous Galerkin discretizations, Commun. Appl. Math. Comput. Sci. 13 (1) (2018) 27–51.

[28] A. Cangiani, Z. Dong, E. Georgoulis, Hp-version discontinuous Galerkin methods on essentially arbitrarily-shaped elements, Math. Comput. 91 (333) (2022) 1–35.

[29] K. Lipnikov, D. Vassilev, I. Yotov, Discontinuous Galerkin and mimetic finite difference methods for coupled Stokes–Darcy flows on polygonal and polyhedral grids, Numer. Math. 126 (2) (2014) 321–360.

[30] P.F. Antonietti, C. Facciola, P. Houston, I. Mazzieri, G. Pennesi, M. Verani, High–order discontinuous Galerkin methods on polyhedral grids for geophysical applications: seismic wave propagation and fractured reservoir simulations, in: Polyhedral Methods in Geosciences, 2021, pp. 159–225.

[31] P.F. Antonietti, M. Botti, I. Mazzieri, S.N. Poltri, A high-order discontinuous Galerkin method for the poro-elasto-acoustic problem on polygonal and polyhedral grids, SIAM J. Sci. Comput. 44 (1) (2022) B1–B28.

[32] B. Cockburn, G. Kanschat, D. Schötzau, C. Schwab, Local discontinuous Galerkin methods for the Stokes system, SIAM J. Numer. Anal. 40 (1) (2002) 319–343.

[33] D. Di Pietro, A. Ern, Discrete functional analysis tools for discontinuous Galerkin methods with application to the incompressible Navier–Stokes equations, Math. Comput. 79 (271) (2010) 1303–1330.

[34] D. Wirasaet, E. Kubatko, C. Michoski, S. Tanaka, J. Westerink, C. Dawson, Discontinuous Galerkin methods with nodal and hybrid modal/nodal triangular, quadrilateral, and polygonal elements for nonlinear shallow water flow, Comput. Methods Appl. Mech. Eng. 270 (2014) 113–149.

[35] P. Antonietti, M. Verani, C. Vergara, S. Zonca, Numerical solution of fluid-structure interaction problems by means of a high order discontinuous Galerkin method on polygonal grids, Finite Elem. Anal. Des. 159 (2019) 1–14.

[36] X. Ye, S. Zhang, A conforming discontinuous Galerkin finite element method for the Stokes problem on polytopal meshes, Int. J. Numer. Methods Fluids 93 (6) (2021) 1913–1928.

[37] S. Zonca, P.F. Antonietti, C. Vergara, A polygonal discontinuous Galerkin formulation for contact mechanics in fluid-structure interaction problems, Commun. Comput. Phys. 30 (1) (2021) 1–33.

[38] M. Corti, P.F. Antonietti, L. Dede', A.M. Quarteroni, Numerical modelling of the brain poromechanics by high-order discontinuous Galerkin methods, Math. Models Appl. Sci. 33 (8) (2023) 1577–1609.

[39] P.F. Antonietti, S. Bonetti, M. Botti, Discontinuous Galerkin approximation of the fully coupled thermo-poroelastic problem, SIAM J. Sci. Comput. 45 (2) (2023) A621–A645.

[40] P.F. Antonietti, L. Mascotto, M. Verani, S. Zonca, Stability analysis of polytopic discontinuous Galerkin approximations of the Stokes problem with applications to fluid–structure interaction problems, J. Sci. Comput. 90 (2022) 1–31.

[41] J.J. Lee, E. Piersanti, K.-A. Mardal, M.E. Rognes, A mixed finite element method for nearly incompressible multiple-network poroelasticity, SIAM J. Sci. Comput. 41 (2) (2019) A722–A747.

[42] M. Causemann, V. Vinje, M.E. Rognes, Human intracranial pulsatility during the cardiac cycle: a computational modelling framework, Fluids Barriers CNS 19 (1) (2022) 1–17.

[43] K.E. Holter, B. Kehlet, A. Devor, T.J. Sejnowski, A.M. Dale, S.W. Omholt, O.P. Ottersen, E.A. Nagelhus, K.-A. Mardal, K.H. Pettersen, Interstitial solute transport in 3d reconstructed neuropil occurs by diffusion rather than bulk flow, Proc. Natl. Acad. Sci. 114 (37) (2017) 9894–9899.

[44] J. Tithof, K.A. Boster, P.A. Bork, M. Nedergaard, J.H. Thomas, D.H. Kelley, A network model of glymphatic flow under different experimentally-motivated parametric scenarios, iScience 25 (5) (2022).

[45] N.J. Abbott, A.A. Patabendige, D.E. Dolman, S.R. Yusof, D.J. Begley, Structure and function of the blood–brain barrier, Neurobiol. Dis. 37 (1) (2010) 13–25.

[46] R. Daneman, A. Prat, The blood–brain barrier, Cold Spring Harb. Perspect. Biol. 7 (1) (2015) a020412.

[47] A. Mikelic, W. Jäger, On the interface boundary condition of Beavers, Joseph, and Saffman, SIAM J. Appl. Math. 60 (4) (2000) 1111–1127.

[48] P.F. Antonietti, S. Giani, P. Houston, Hp-version composite discontinuous Galerkin methods for elliptic problems on complicated domains, SIAM J. Sci. Comput. 35 (3) (2013) A1417–A1439.

[49] E.M. Stein, Singular Integrals and Differentiability Properties of Functions, Princeton University Press, 1970.

[50] P. Antonietti, I. Mazzieri, High-order discontinuous Galerkin methods for the elastodynamics equation on polygonal and polyhedral meshes, Comput. Methods Appl. Mech. Eng. 342 (2018) 414–437.

[51] P.F. Antonietti, S. Bonetti, M. Botti, M. Corti, I. Fumagalli, I. Mazzieri, Lymph: an efficient high-order solver for differential problems with polytopal discontinuous Galerkin methods, submitted for publication. arXiv preprint, arXiv:2401.13376, 2023.

[52] P.J. LaMontagne, T.L. Benzinger, J.C. Morris, S. Keefe, R. Hornbeck, C. Xiong, E. Grant, J. Hassenstab, K. Moulder, A.G. Vlassenko, M.E. Raichle, C. Cruchaga, D. Marcus, OASIS-3: longitudinal neuroimaging, clinical, and cognitive dataset for normal aging and Alzheimer disease, medRxiv 2019.12.13.19014902, 2019.

[53] B. Fischl, Freesurfer, NeuroImage 62 (2) (2012) 774–781.

[54] L. Antiga, M. Piccinelli, L. Botti, B. Ene-Iordache, A. Remuzzi, D.A. Steinman, An image-based modeling framework for patient-specific computational hemodynamics, Med. Biol. Eng. Comput. 46 (2008) 1097–1112.

[55] G. Karypis, K. Schloegel, V. Kumar, Parmetis: Parallel graph partitioning and sparse matrix ordering library, University of Minnesota, 1997, TR 97–060.

[56] O. Balédent, I. Idy-peretti, et al., Cerebrospinal fluid dynamics and relation with blood flow: a magnetic resonance study with semiautomated cerebrospinal fluid segmentation, Invest. Radiol. 36 (7) (2001) 368–377.

[57] S.H. Pahlavian, J. Oshinski, X. Zhong, F. Loth, R. Amini, Regional quantification of brain tissue strain using displacement-encoding with stimulated echoes magnetic resonance imaging, J. Biomech. Eng. 140 (8) (2018) 081010.

[58] L.A. Mihai, S. Budday, G.A. Holzapfel, E. Kuhl, A. Goriely, A family of hyperelastic models for human brain tissue, J. Mech. Phys. Solids 106 (2017) 60–79.

[59] S. Budday, G. Sommer, J. Haybaeck, P. Steinmann, G.A. Holzapfel, E. Kuhl, Rheological characterization of human brain tissue, Acta Biomater. 60 (2017) 315–329.

[60] A. Anssari-Benam, M. Destrade, G. Saccomandi, Modelling brain tissue elasticity with the Ogden model and an alternative family of constitutive models, Philos. Trans. R. Soc. A 380 (2234) (2022) 20210325.

[61] A. Quarteroni, L. Dede', A. Manzoni, C. Vergara, Mathematical Modelling of the Human Cardiovascular System: Data, Numerical Approximation, Clinical Applications, vol. 33, Cambridge University Press, 2019.

[62] L. Feng, H. Gao, B. Griffith, S. Niederer, X. Luo, Analysis of a coupled fluid-structure interaction model of the left atrium and mitral valve, Int. J. Numer. Methods Biomed. Eng. 35 (11) (2019) e3254.

[63] M. Hirschhorn, V. Tchantchaleishvili, R. Stevens, J. Rossano, A. Throckmorton, Fluid–structure interaction modeling in cardiovascular medicine–a systematic review 2017–2019, Med. Eng. Phys. 78 (2020) 1–13.

[64] M. Bucelli, A. Zingaro, P.C. Africa, I. Fumagalli, L. Dede', A. Quarteroni, A mathematical model that integrates cardiac electrophysiology, mechanics, and fluid dynamics: application to the human left heart, Int. J. Numer. Methods Biomed. Eng. 39 (3) (2023) e3678.

[65] I. Fumagalli, R. Polidori, F. Renzi, L. Fusini, A. Quarteroni, G. Pontone, C. Vergara, Fluid-structure interaction analysis of transcatheter aortic valve implantation, Int. J. Numer. Methods Biomed. Eng. 39 (6) (2023) e3704.

[66] G. Ringstad, L.M. Valnes, A.M. Dale, A.H. Pripp, S.-A.S. Vatnehol, K.E. Emblem, K.-A. Mardal, P.K. Eide, Brain-wide glymphatic enhancement and clearance in humans assessed with MRI, JCI Insight 3 (13) (2018).

[67] K.-A. Mardal, M.E. Rognes, T.B. Thompson, L.M. Valnes, Mathematical Modeling of the Human Brain: from Magnetic Resonance Images to Finite Element Simulation, Springer Nature, 2022.

[68] B. Su, R. San Tan, J. Le Tan, K.W.Q. Guo, J.M. Zhang, S. Leng, X. Zhao, J.C. Allen, L. Zhong, Cardiac MRI based numerical modeling of left ventricular fluid dynamics with mitral valve incorporated, J. Biomech. 49 (7) (2016) 1199–1205.

[69] I. Fumagalli, M. Fedele, C. Vergara, L. Dede', S. Ippolito, F. Nicolò, C. Antona, R. Scrofani, A. Quarteroni, An image-based computational hemodynamics study of the systolic anterior motion of the mitral valve, Comput. Biol. Med. 123 (2020) 103922.

[70] I. Fumagalli, P. Vitullo, C. Vergara, M. Fedele, A.F. Corno, S. Ippolito, R. Scrofani, A. Quarteroni, Image-based computational hemodynamics analysis of systolic obstruction in hypertrophic cardiomyopathy, Front. Physiol. 12 (2022) 787082.

[71] L. Bennati, C. Vergara, V. Giambruno, I. Fumagalli, A.F. Corno, A. Quarteroni, G. Puppini, G.B. Luciani, An image-based computational fluid dynamics study of mitral regurgitation in presence of prolapse, Cardiovasc. Eng. Technol. (2023) 1–19.

[72] O. Baenen, A.C. Carreño-Martínez, T.P. Abraham, S. Rugonyi, Energetics of cardiac blood flow in hypertrophic cardiomyopathy through individualized computational modeling, J. Cardiovasc. Dev. Dis. 10 (10) (2023) 411.

[73] J.D. Jones, P. Castanho, P. Bazira, K. Sanders, Anatomical variations of the circle of Willis and their prevalence, with a focus on the posterior communicating artery: a literature review and meta-analysis, Clin. Anat. 34 (7) (2021) 978–990.

[74] H. Liu, D. Wang, X. Leng, D. Zheng, F. Chen, L.K.S. Wong, L. Shi, T.W.H. Leung, State-of-the-art computational models of circle of Willis with physiological applications: a review, IEEE Access 8 (2020) 156261–156273.

[75] M. Corti, F. Bonizzoni, P.F. Antonietti, Structure preserving polytopal discontinuous Galerkin methods for the numerical modeling of neurodegenerative diseases, arXiv preprint, arXiv:2308.00547, 2023.

[76] M. Corti, F. Bonizzoni, L. Dede', A.M. Quarteroni, P.F. Antonietti, Discontinuous Galerkin methods for Fisher–Kolmogorov equation with application to *alpha*-synuclein spreading in Parkinson's disease, Comput. Methods Appl. Mech. Eng. 417 (2023) 116450.